FINITE ELEMENT ANALYSIS OF OZ SAFEROOM

A TECHNICAL REPORT SUBMITTED TO

OZ SAFEROOMS, DEL CITY, OK.

BY

YEVGENIY PARFILKO

FERNANDO AMARAL DE ARRUDA

DR. BENJAMIN VARELA

ROCHESTER INSTITUTE OF TECHNOLOGY

APRIL 2017

Abstract

Explicit dynamic Finite Element Analysis were performed on a reinforced concrete OZ saferoom to evaluate its performance under impact from tornado-generated debris and tornado-dragged vehicles. Tests were structured to comply with NSSA testing specifications.

This report is split into five sections. The first four sections examine simplified components of the shelter subjected to various debris impact. The last section examines the collision of a vehicle into the full-scale saferoom. For the debris impact simulations, frontal and corner impacts were examined to identify the extent of damage from soft and hard missiles. Damage was also examined for the sliding door structure. For the vehicle crash, isolated side-wall and roof impacts were examined to identify the extent of damage in different wall geometries. A full-scale impact scenario was then modeled in order to investigate the dynamic response of the whole structure.

The debris simulations show that soft impacts typically cause the most damage only to the exterior surface of the concrete at the point of impact, with comparatively little spallation effects. This differs from the plug-formation seen in hard impacts. Repeated impacts result in accumulated damage that eventually results in perforation, or piercing, of the structure. The crash analyses show that the vehicle behaves like a soft projectile, unless the engine block hits the wall. Results indicate good performance of the structure at slow collision speeds and spalling when subject to high speeds.

This report covers 32 simulations. All files may be found on the included thumb drive. Simulations are separated into folders by sections, following the same section numbering scheme as the report.

Contents

Introduction and History

Structures are typically designed to withstand two types of loading: distributed loads such as wind loads, or high-energy hard impacts such as steel projectiles. Saferooms that protect against severe storms such as tornadoes are affected by a third type of loading - soft impacts caused by windborne debris. This can include wood beams torn from houses and beams swept up from industrial structures. In the most extreme cases, a car can be accelerated by high-speed winds. Predicting the damage from soft impacts and the long-term effect on the structure is a difficult task.

A Finite Element Model is the best tool available to solve this type of problem. The industry standard software for impact analysis is LS-DYNA, a finite element solver used to predict the dynamic deformation for complex materials and structures under sudden loading. It is used in the automotive industry to model vehicle collisions as well as concrete roadside safety structures, and in the aerospace industry to model crash scenarios. LS-DYNA seemed appropriate and necessary to achieve the numerical accuracy that was desired in these simulations. In addition to the LS-DYNA solver, ANSYS software suite was used to import and mesh geometries of complex structures. The results were exported to LS-DYNA, where material models and boundary conditions were imposed, and the mechanical system was solved. All figures, tables and charts in the following report are reproduced from these programs, and are included in the external drive.

Before the finite element method became commercially widespread, various empirical formulas were used to predict penetration of projectiles into concrete. Throughout this report, two formulas are used to validate simulation results, and to show unexpected behavior.

EMPIRICAL METHODS

In the 1950s, the National Defense Research Committee (NDRC) developed and refined a formula for ballistic missile penetration. This formula was empirically derived from extensive test data from impact of a steel missile into a very thick concrete slab. The formula is widely applicable and shows good agreement with a variety of subsequent simulations and experiments. The formula is shown in Equation 1, and is henceforth referred to as the NDRC formula or the NDRC equation.

$$G\left(\frac{x}{d}\right) = \frac{180}{(f_c')^{0.5}}\ N\ D\ d^{0.2}\left(\frac{V_0}{1000}\right)^{1.8} = \begin{cases} (\frac{x}{2d})^2\ for\ \frac{x}{d} < 2 \\ \frac{x}{d} - 1\ for\ \frac{x}{d} \geq 2 \end{cases} \quad \ldots\ldots\ldots\ldots\ldots\ldots (1)$$

f_c'	(psi)	unconfined compressive strength
V_0	(ft/s)	initial impact velocity
D	$(-)$	damage scaling factor
d	(in)	missile diameter
N	$(-)$	missile nose cone shape factor

In 1981, consulting engineer A. K. Kar modified the NDRC formula for tornado-generated missiles. A scaling factor was added based on the hardness of the material relative to steel, which gave results for softer materials at lower speeds. Empirical terms were substantiated by experimental data. The formula is given by Equation 2, it is henceforth referred to as the Kar formula.

$$G\left(\frac{x}{d}\right) = \frac{180}{(f_c')^{0.5}}\ \left(\frac{E}{E_m}\right)^{1.25}\ \frac{W\ N_2}{D\ d^{1.8}}\left(\frac{V_0}{1000}\right)^{1.8} = \begin{cases} (\frac{x}{2d})^2\ for\ \frac{x}{d} < 2 \\ \frac{x}{d} - 1\ for\ \frac{x}{d} \geq 2 \end{cases} \quad \ldots\ldots\ldots\ldots\ldots\ldots (2)$$

E	(psi)	material elastic modulus
W	(lb)	missile weight

The advantage to using these formulas is that they offer close-form predictions for the missile penetrations. Each formula takes as its input only simple material properties that are known in advance, as well as missile speed, weight, and area, which are readily obtained from the NSSA Standard. Thus, the NDRC and Kar Formulas can then be used to as a direct comparison to the deflection results given by the simulation.

NUMERICAL METHODS

Unlike empirical formulas, numerical material models implicitly predict the behavior of materials by tracking stress and strain time histories within a single element, and assembling the elements to form the global geometry. These material models are built into solvers such as LS-DYNA and ANSYS. Although they are computationally intensive, they capture a range of information about the material, including nonlinear properties such as rate-dependent hardening or damage formulation. These properties can then be visualized directly on the desired geometry.

In this report, the Riedel-Hermaier-Thoma (RHT) model was used predominantly. The RHT model is a standard material in the LS-DYNA material library, and can be used in conjunction with steel reinforcement. This model accurately represents the compressive, shear, and tensile properties of concrete, and allows for damage from an impact to be visualized. A visual of residual damage at the end of an impact is often included in the results section of the report. This graphic is obtained from the RHT damage variable.

In addition to RHT, the CSCM model is sometimes used within this report. The Continuous Surface Cap Model (CSCM) for concrete was originally developed at the Federal High-Way Administration as a material for road surfaces and barriers. The CSCM model has the ability to accurately show element erosion (or chipping) patterns in concrete. Furthermore, the material can be pre-damaged using a variable parameter, which is useful for examining cases where concrete may be more fragile and subject to failure. Henceforth, a numerical model of concrete may be referred to as RHT or CSCM concrete, respectively.

SECTION 1: FRONTAL IMPACT

The frontal impact simulation is a direct adaptation of the Debris Impact Test described in the 2009 ICC/NSSA Standard. The goal was to show that even 6" unreinforced concrete can completely absorb damage from a 15-lb wood missile travelling at 100 mph. High-strength concrete (5800 psi) was chosen for the test to mimic OZ saferoom materials. Various test dimensions and parameters were also adapted from experimental tests to make the results easily comparable. Slab dimensions, projectile speed, and frontal area of the projectile were adapted from the NSSA Standard for storm shelter tests, while concrete properties and slab thickness were given by the sponsor, OZ Saferooms. The full list of simulation parameters is given in Table 1.1.1.

Table 1.1.1 - Major model and material parameters for simulation series 1.

Group	Name	Value	Unit	Source	Notes
Slab	Width	1200	mm	NSSA	Converted to metric
Slab	Height	1200	mm	NSSA	Converted to metric
Slab	Thickness	150	mm	OZ	Converted to metric
Slab	Rebar	#4	Gauge	OZ	Converted to 12.7mm OD
Projectile	Mass	6.8	kg	NSSA	Converted to metric
Projectile	Frontal Area	3378.1	mm^2	NSSA	Converted to metric
Projectile	Length	variable	mm	None	Det. by mass and density
Projectile	Initial Velocity	45	m/s	NSSA	Approximately 100mph
Mat'l Prop	Wood density	500	kg/m^3	None	Approximate value
Mat'l Prop	Concrete density	2000	kg/m^3	None	Approximate value
Mat'l Prop	Concrete strength	34.5	MPa	OZ	High-strength concrete

In accordance with the NSSA test, a wood projectile was "fired" into a 4'x4' slab of the protective material, concrete, and the dynamic response was analyzed. The general test setup is shown in Figure 1.1.1; further test geometries differ only in the location of impact. In addition to the basic impact at three locations, this test examined the effects of moisture and temperature on the wood-concrete interaction. The list of simulations is given in Table 1.1.2.

Table 1.1.2 - List of series 1 simulation names and descriptions.

Test No.	Test Name	Date Run	Description
1.1	front	8/14/2014	NSSA Debris Impact Simulation
1.2	edge	8/14/2014	NSSA DIS at location #2
1.3	corner	8/14/2014	NSSA DIS at location #3
1.4	M0.T0	7/30/2014	moisture 0% temperature 0C
1.5	M0.T30	7/30/2014	moisture 0% temperature 30C
1.6	M20.T30	7/30/2014	moisture 20% temperature 30C
1.7	M100.T30	7/30/2014	moisture 100% temperature 30C
1.81	V20	9/30/2014	Front impact at 20 m/s (45 mph)
1.82	V30	9/30/2014	Front impact at 30 m/s (65 mph)
1.83	V40	9/30/2014	Front impact at 40 m/s (90 mph)
1.84	V50	9/30/2014	Front impact at 50 m/s (110 mph)
1.85	V60	9/30/2014	Front impact at 60 m/s (135 mph)
1.86	V80	9/30/2014	Front impact at 80 m/s (180 mph)
1.87	V100	9/30/2014	Front impact at 100 m/s (225 mph)
1.88	V120	9/30/2014	Front impact at 120 m/s (270 mph)
1.89	V150	9/30/2014	Front impact at 150 m/s (335 mph)

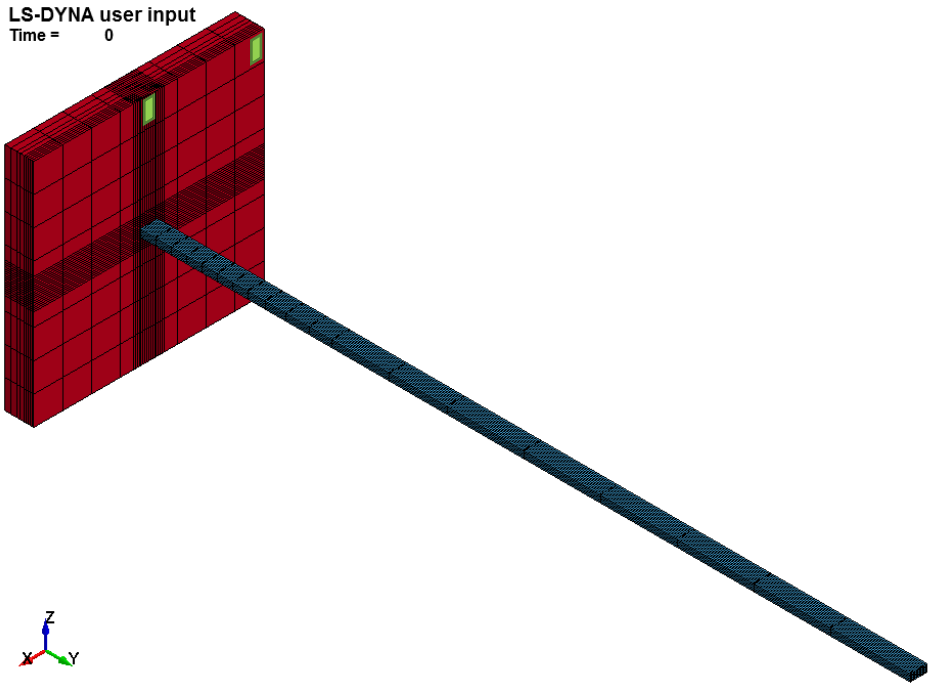

Figure 1.1.1 – General simulation setup for series 1 tests. A wood stud impacts a 6”-thick concrete slab at the specified initial velocity. The slab is unreinforced, and constrained at the sides. The green rectangles designate the locations of the edge and corner impacts.

RESULTS

Tests geometries were created and meshed in ANSYS Workbench, and solved in LS-DYNA. Some initial work was done to characterize mesh dependency and select appropriate sizing and units for the simulations. After optimization, tests typically completed in just a few minutes. The wood missile was safely deflected in all simulations, with only minor local damage to the concrete.

At 100 mph initial velocity, the damage crater was about 10mm deep and slightly larger than the missile in diameter. The damage crater shape and dynamic deflection was independent of the location of impact, leading to the conclusion that the dynamics of soft impacts of this nature only affect a small area, and are independent of boundary conditions or stresses far away. Figure 1.1.2 shows the final deflections of nodes in the impact region, and Figures 1.1.3-1.1.5 show the nodal displacement, acceleration, and strains. This data is also summarized in Table 1.1.3.

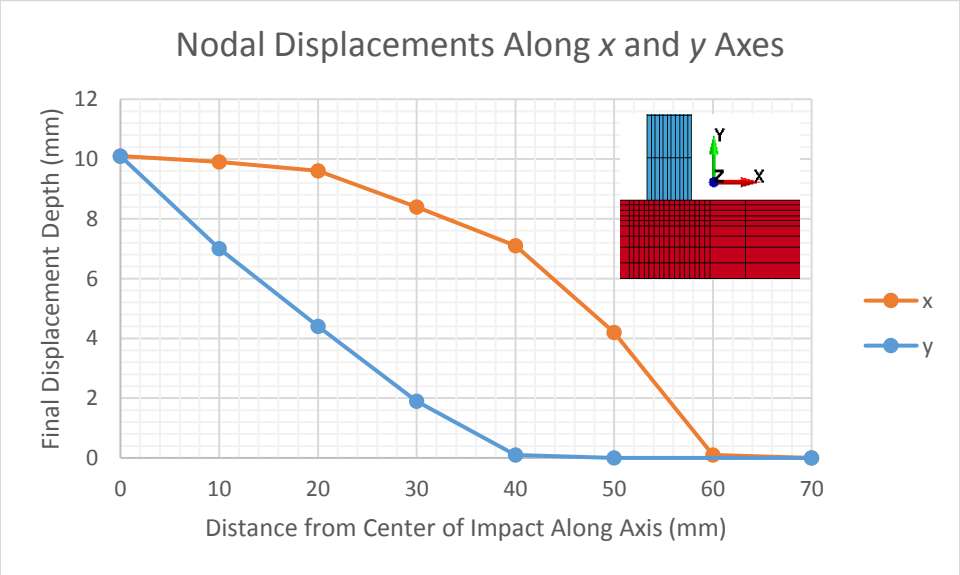

Figure 1.1.2 - Displacement depth at various nodes in the impact region for simulation 1.1. As distance from the impact center decreases, displacements tend to zero. Note the missile radius is approximately 45 mm, and the affected region extends roughly 45mm into the concrete.

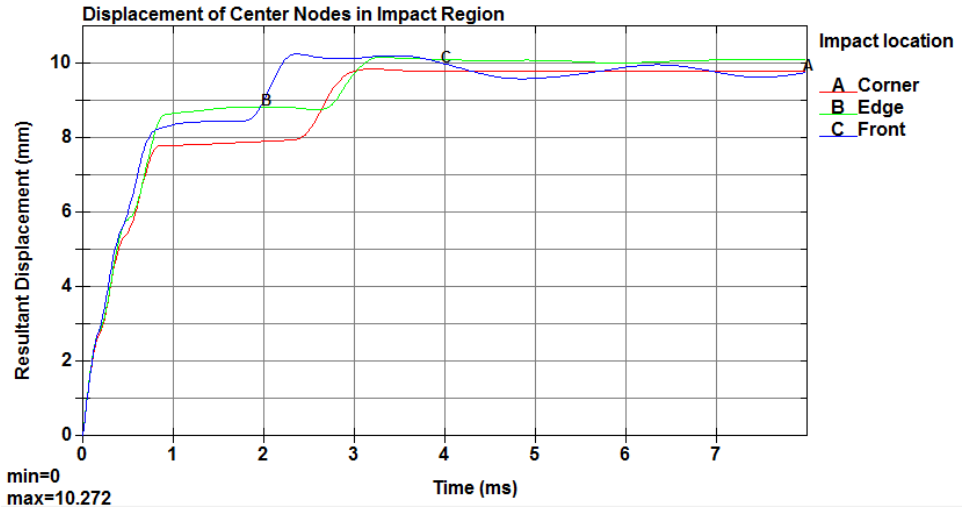

Figure 1.1.3 - Nodal displacements for simulations 1.1, 1.2, and 1.3. Note the vibrational response of the slab (seen in node C) disappears when the impact occurs at the boundary.

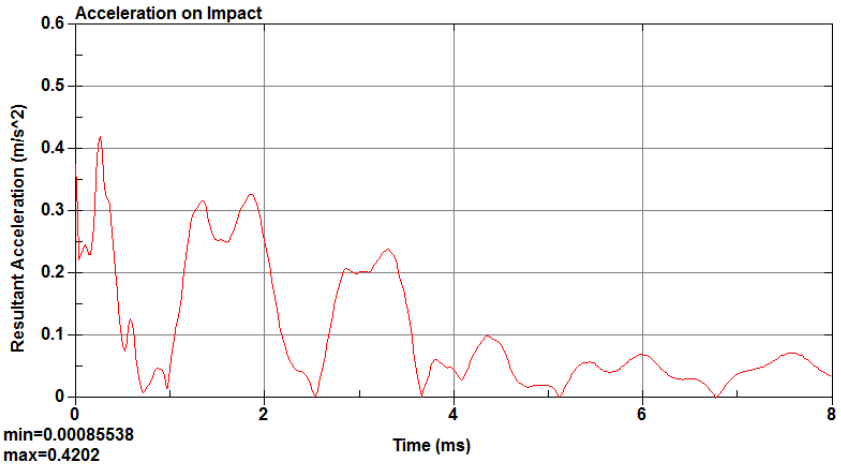

Figure 1.1.4 – Rigid body acceleration for simulation 1.1.

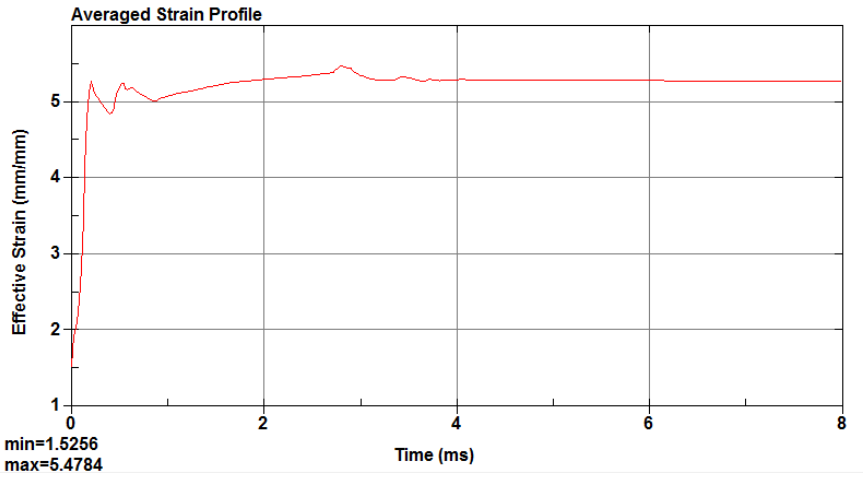

Figure 1.1.5 – Strain profile for simulation 1.1.

Table 3 - Summary of results for simulations 1.1-1.3.

Metric	Units	Front	Corner	Edge
Max. Displacement	mm	10.3	10.1	9.8
Max. Acceleration	m/s^2	0.40	1.24	0.38
Avg. Plastic Strain	mm/mm	0.21	0.21	0.21
Damage area	cm^2	55	55	55
Damage Depth	mm	35	35	35

Environmental variables such as atmospheric temperature and moisture content were taken into consideration. Tests 1.4-1.7 examine the dynamic response for different combinations of temperature and moisture. The displacement paths are shown in Figure 1.1.4. The diagram confirms that strain rates and energy absorption vary only slightly over a wide range of environmental variables. Further tests were conducted at 0% Moisture and 0 degrees Celsius (material default) with the understanding that transferred momentum can vary up to +10%.

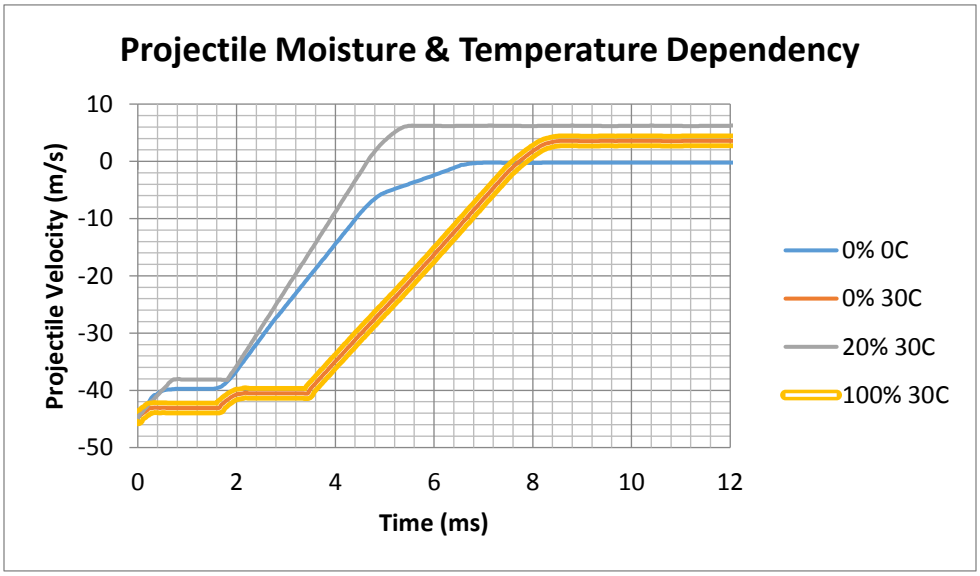

Figure 1.1.4 - Velocity time histories for projectiles in tests 1.4-1.7. Variations in temperature and moisture of the wood will cause some variation in the rate of momentum transfer and erosion of wood elements. Additionally, wood at higher temperatures tends to "spring back".

A final series of tests 1.8X was conducted to track how the penetration depth varied as a function of impact speed. The NDRC and Kar empirical formulas were included as benchmarks of previous work. The test series data is plotted in Figure 1.1.5.

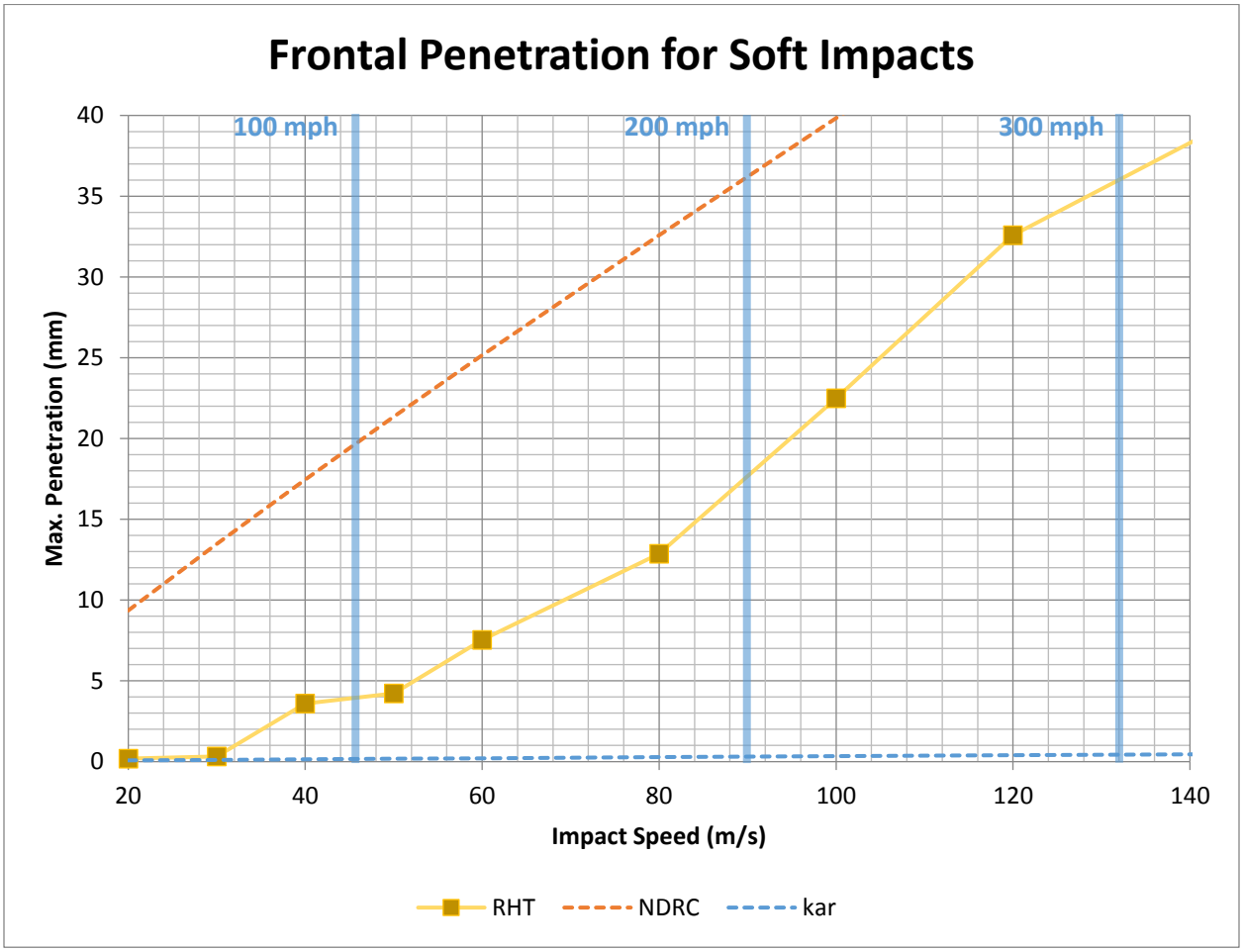

Figure 1.1.5 - Calibration curve for simulations 1.81-1.89. The RHT test series is shown in yellow, the NDRC equation in orange, and the Kar equation in blue. The vertical blue bars give the speed in miles per hour. Penetration depth was taken as an average of three nodes in the impact region, rather than the maximum nodal deformation.

Even at a thickness of 6", OZ concrete is strong enough to withstand impacts in excess of 300 mph without breaking, though some spallation is expected for impacts in excess of 100 mph. Also, the penetration depth for the simulations falls between the NDRC and Kar predictions, implying a transition region between soft and hard impacts.

SECTION 2: FRONTAL STEEL IMPACT

The soft impacts conducted in the first series of simulations gave promising results, and the scope of the project was accordingly expanded to take into account heavier and denser missiles. These impacts would cover the less common cases of a tornado saferoom being struck by a metal beam, commonly found in industrial structures such as fences, signs, water towers, industrial scaffolding, etc. and will further increase the confidence in the safety of the structure.

Series 2 simulations cover frontal impacts from hard projectiles. The concrete geometry and properties are unchanged, but the wood missile is substituted with an I-beam supplied by Grainger Inc. The particular product was selected because of its commercial popularity, indicating common usage. Additionally, the I-beam had a similar frontal area to the wood stud, so that the tests would agree qualitatively as well as quantitatively. Simulation parameters are tabulated below.

Table 2.1.1 - Model and material parameters for simulation series 2.

Group	Name	Value	Unit	Source	Notes
Slab	Width	1200	mm	NSSA	Converted to metric
Slab	Height	1200	mm	NSSA	Converted to metric
Slab	Thickness	150	mm	OZ	Converted to metric
Slab	Rebar	#4	Gauge	OZ	Converted to 12.7mm OD
Projectile	Mass	15.49	kg	Grainger	
Projectile	Frontal Area	4510	mm^2	Grainger	
Projectile	Contact Area	1080	mm^2	Grainger	
Projectile	Length	1829	mm	Grainger	
Mat'l Prop	Steel density	7850	kg/m^3	ASTM	
Mat'l Prop	Concrete density	2000	kg/m^3	None	Approximate value
Mat'l Prop	Concrete strength	34.5	MPa	OZ	High-strength concrete

The steel projectile chosen was significantly heavier than the wood missile, so the simulation was adjusted to account for the extra mass. To preserve the constraint of equal kinetic energy, the impact speed was reduced to 19.2 m/s. Figure 2.1.1 shows the generic setup of the finite element model.

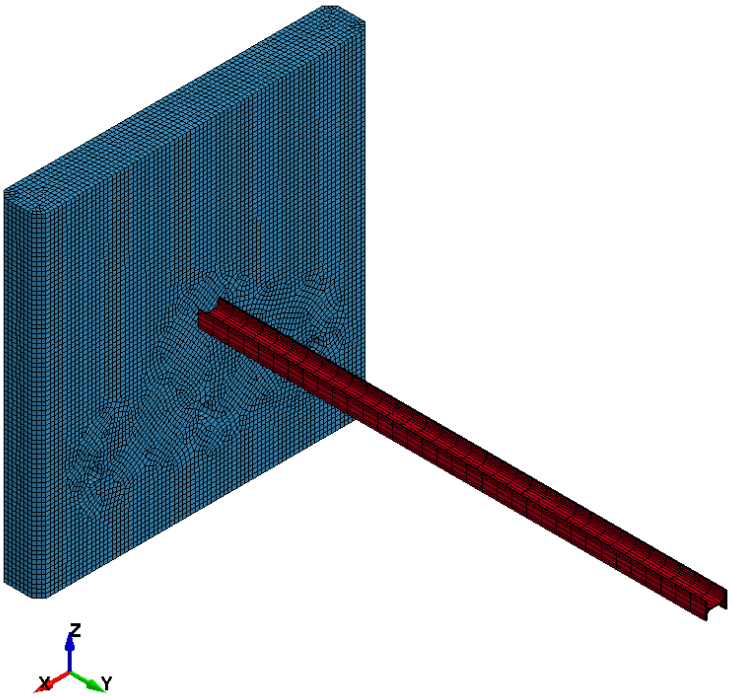

Figure 2.1.1 - Model setup for series 2 simulations showing meshes for refined slab and steel I-beam.

RESULTS

The simulation time history showed that even though the steel beam is deflected, elastoplastic deformation occurs throughout the thickness of the slab. The initial stages of plug formation can also be visualized in a cross section view, as shown in in Figure 2.1.2.

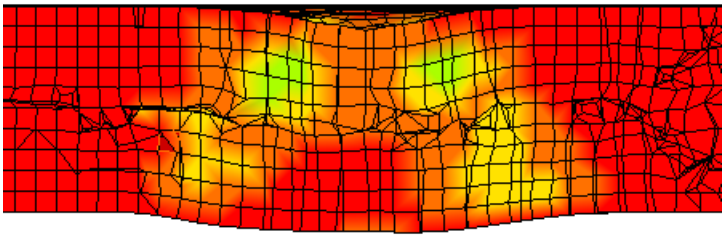

Figure 2.1.2 –Third principal stress revealing early signs of plug formation. High stress shown in green and blue.

The simulated deformation is also in close agreement with the NDRC formula predictions. The simulation showed a penetration of 12.41 mm, and the formula predicted 12.19 mm. The results agree within the 5% margin of error given by the assumptions made in the NDRC formula. Compared to the soft impact, the hard impact penetration is slightly higher. This is because the net energy absorbed by the concrete was the same, with some variation due to strain hardening effects. Figure 2.1.3 illustrates how the soft impact resulted in loading-unloading cycles, while the hard impact resulted in continuous deformation. Figure 2.1.4 shows the acceleration time history.

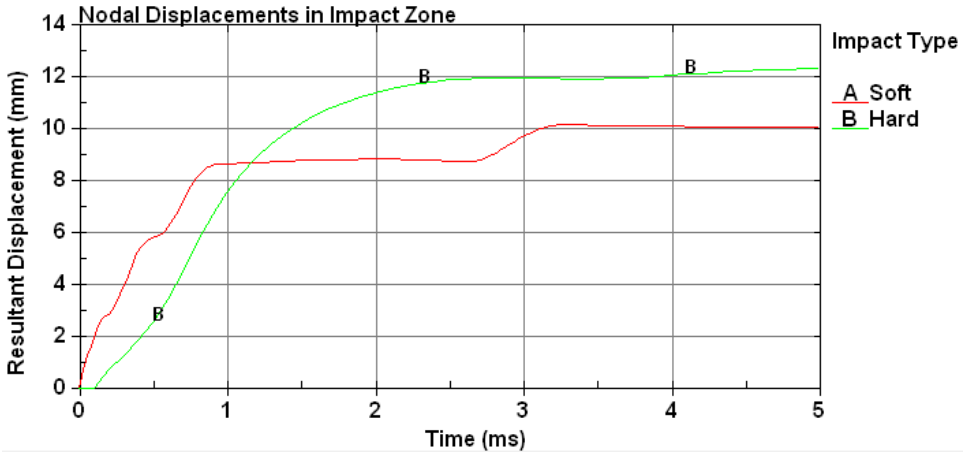

Figure 2.1.3 - Comparison plot of soft and hard impacts. Note that initial kinetic energy and strain rate are the same for each simulation, but the hard impact results in deeper penetration.

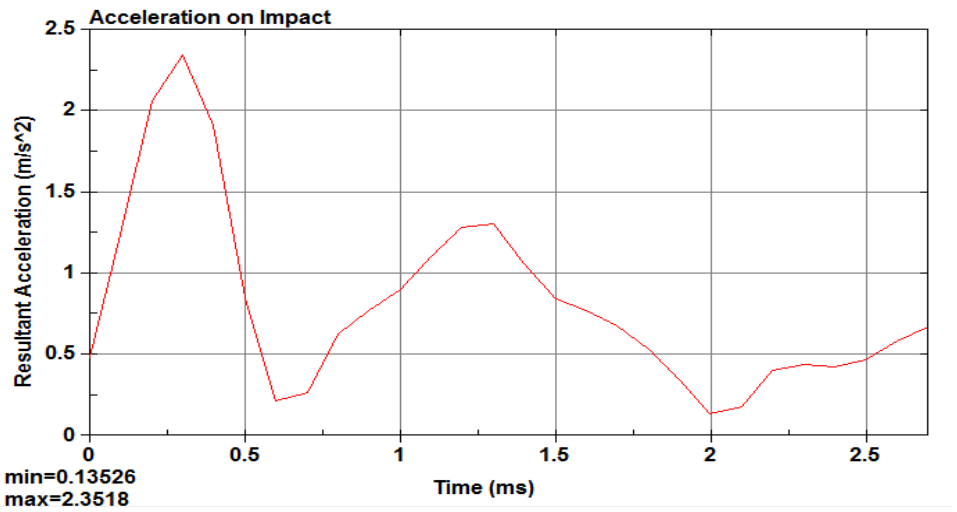

Figure 2.1.4- Acceleration plot for simulation 2.1.

SECTION 3: CORNER IMPACT

The corner of the saferoom presented the weakest part of the concrete structure because of limited support and lack of reinforcement at the corner. Additionally, the failure mode of the concrete is in shear rather than tension or compression. Therefore, the corner in particular required thorough evaluation. In order to effectively characterize multimodal concrete failure, the CSCM Concrete material was implemented in addition to the RHT material. Both models utilize a continuous compressive cap yield surface, but formulate damage differently. Studying both material models will yield helpful insight into a realistic measure of damage for concrete.

Table 3.1.1 - Table of simulation parameters, adapted from series 1.

Group	Name	Value	Unit	Source	Notes
Slab	Width	1200	mm	NSSA	Converted to metric
Slab	Height	1200	mm	NSSA	Converted to metric
Slab	Thickness	150	mm	OZ	Converted to metric
Slab	Rebar	#4	Gauge	OZ	Converted to 12.7mm OD
Projectile	Mass	6.8	kg	NSSA	Converted to metric
Projectile	Frontal Area	3378.1	mm^2	NSSA	Converted to metric
Projectile	Length	variable	mm	None	Det. by mass and density
Projectile	Initial Velocity	45	m/s	NSSA	Approximately 100mph
Mat'l Prop	Wood density	500	kg/m^3	None	Tentative value
Mat'l Prop	Concrete density	2000	kg/m^3	None	Tentative value
Mat'l Prop	Concrete strength	34.5	MPa	OZ	High-strength concrete

Table 3.1.2 - Table of simulations for test series 3.

Test No.	Test Name	Date Run	Description
3.1	corner	9/24/2014	adapted soft impact 2 cm away from free surface
3.2	edge	9/25/2014	Corner test with stud center over edge
3.3	edge rht er120	9/26/2014	edge test with erosion parameter set to 120%
3.4	edge cscm pre50	9/26/2014	edge test with CSCM material and 50% predamage

Simulation series 3 examined four corner impact scenarios: A frontal impact in the vicinity of a free edge, an impact on a free edge, and an impact with predamaged concrete in RHT and CSCM materials. The simulation geometry was the same in each case and is shown in Figure 3.1.1 below.

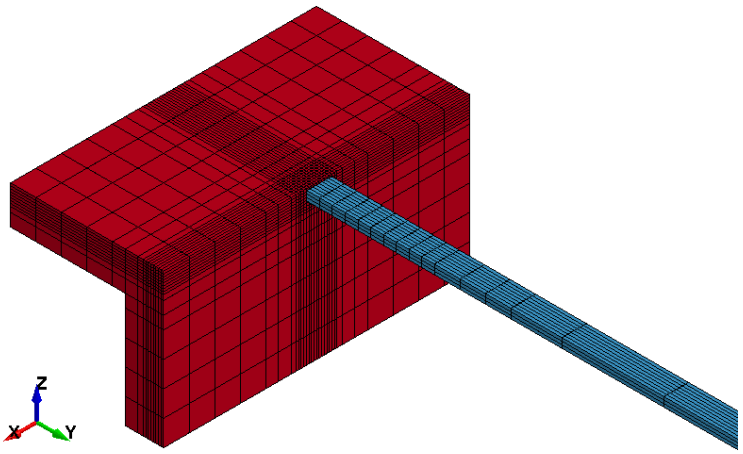

Figure 3.1.1 - Simulation geometry and mesh for series 3 tests. A custom sizing function for the mesh was used.

RESULTS

Generally, impacts near the corner yielded the same impact profile as the frontal impact, demonstrating that the soft impact characterization is relevant for geometries with one or more free surfaces. As the face of the projectile was moved directly over the edge, the impact profile changed, with asymmetrical deformation occurring and the projectile deflecting.

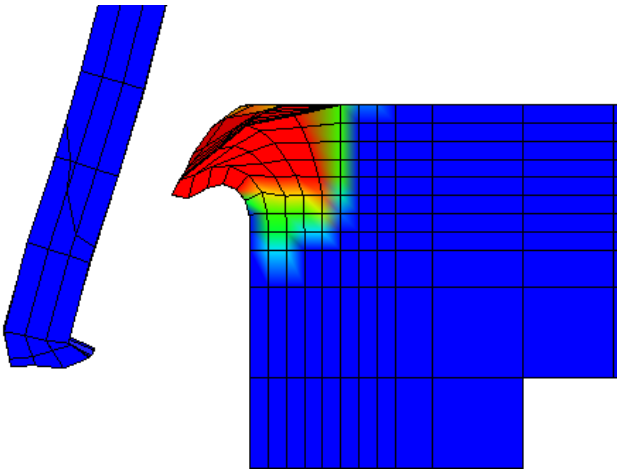

Figure 3.1.2 - Cross section of the impact region showing projectile deflection and damage accumulation.

Table 3.1.3 - Table of summarized results for simulations 3.1-3.4.

Metric	Units	Corner	Edge	RHT120	CSCM50
Max. Displacement	mm	2.4	65.8	47.2	16.6
Max. Acceleration	m/s^2	0.34	0.35	0.35	0.39
Avg. Plastic Strain	mm/mm	0.21	0.88	0.90	0.94
Damage area	cm^2	50	60	60	60
Damage Depth	mm	25	45	45	50

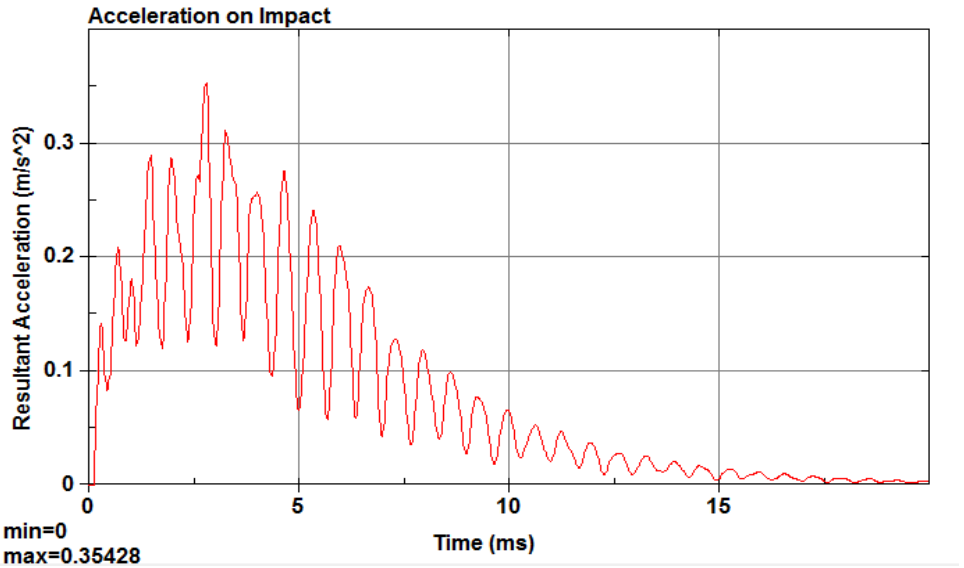

Figure 3.2.1 - Rigid body acceleration for simulation 3.2.

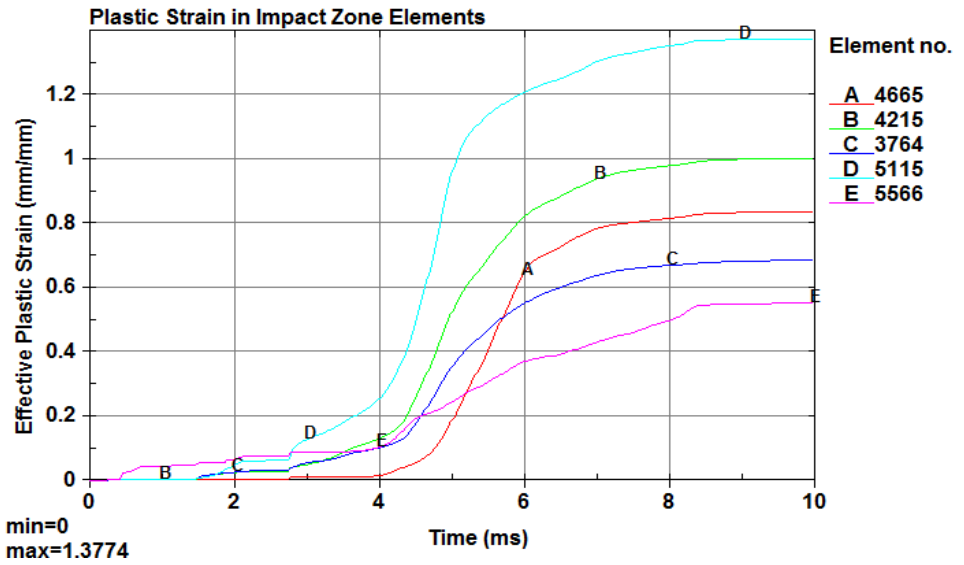

Figure 3.2.2 – Several strain profiles in the impact zone for simulation 3.2.

Figure 3.1.2 shows the cross section of the concrete after the missile has deflected. Both internal damage and plastic deformation occur. The results of each simulation ate given in Table 3.1.3, with responses from a specific test shown in Figures 3.2.1 and 3.2.2. Figure 3.3.1 shows a side-by-side comparison of corner impacts with pre-damaged RHT and CSCM models. In both cases plastic deformation occurs, with a deflection of the missile and a 40% reduction in velocity (65% energy reduction). CSCM includes an internal parameter for pre-damage while RHT is weakened by reducing the strain criterion for erosion.

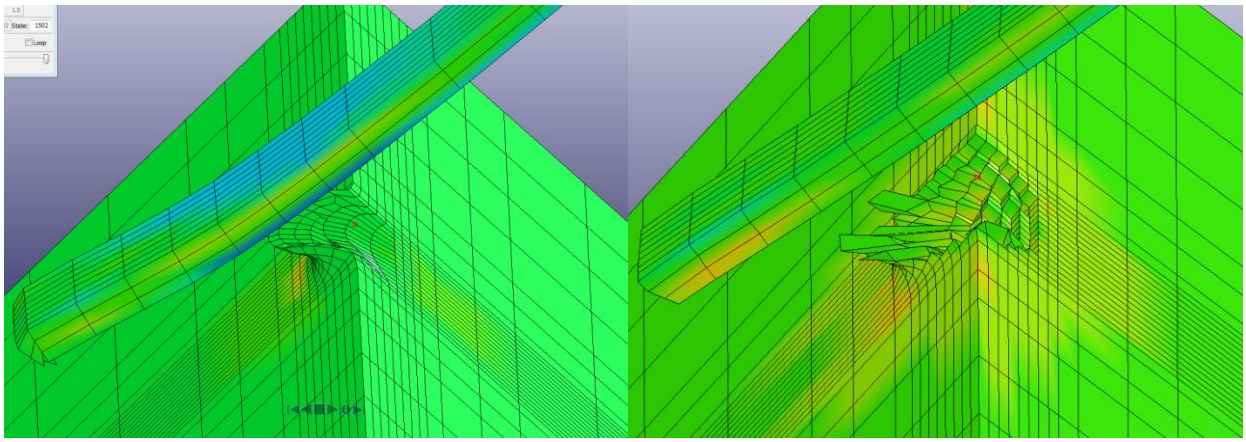

Figure 3.3.1 - Corner impact test visualizations. RHT is on the left and CSCM is on the right.

Corner impacts result in higher damage and deformation than normally expected, but have less of a chance to end in perforation of the saferoom wall. Plastic strains for edge impacts tend to be several times higher than those seen in frontal impacts. In the case of a corner impact, penetration depth cannot be predicted with the NDRC or Kar formulas. Rather, the depth of the impact zone is the same as the width, which has been previously determined to be 150% to 200% of the missile diameter, depending on whether full or partial damage was considered. In practice, chamfered corners will decrease structural damage, but the effective worst case scenario is considered in this report in order to demonstrate the structural strength of the concrete material itself.

SECTION 4: DOOR IMPACT

The final component test to be run is the door test. Only a single test was run to characterize the impact absorbing qualities of the door. The center point was chosen because it would represent the weakest point, and impacted at 50 m/s. Dimensions of the door and simulation parameters are given in Table 4.1.1.

Table 4.1.1 - Table of simulation parameters for the door impact.

Group	Name	Value	Unit	Source	Notes
Door	Width	914.4	mm	OZ	Converted to metric
Door	Height	1828.8	mm	OZ	Converted to metric
Door	Total Thickness	41.40	mm	OZ	Excludes Bolts
Door	Steel Sheet Thick.	3.30	mm	OZ	Converted to metric
Projectile	Mass	6.8	kg	NSSA	Converted to metric
Projectile	Frontal Area	3378.1	mm^2	NSSA	Converted to metric
Projectile	Length	4000.0	mm	None	Det. by mass and density
Projectile	Initial Velocity	50	m/s	NSSA	Approximately 110mph
Mat'l Prop	Wood density	500	kg/m^3	OZ	
Mat'l Prop	Steel density	7800	kg/m^3	ASTM	1018 Steel assumed
Mat'l Prop	Steel strength	220	MPa	ASTM	1018 Steel assumed

The door was modeled and meshed in ANSYS software, and the final mesh is shown in Figure 4.1.1. The door assembly consists of a layer of plate steel between two wood sheets. The layers are bonded with glue and clamped together with bolts at regular intervals. Rigid constraints were placed along the top and bottom edges of the steel sheet to simulate the rollers to which it would be fixed.

Table 4 – Results table for simulation 4.1.

Metric	Units	Value
Max. Rigid Body Displacement	mm	13.8
Max. Local Displacement	Mm	34.5
Max. Acceleration	m/s^2	603
Max. Plastic Strain (Wood in Impact Area)	mm/mm	0.018

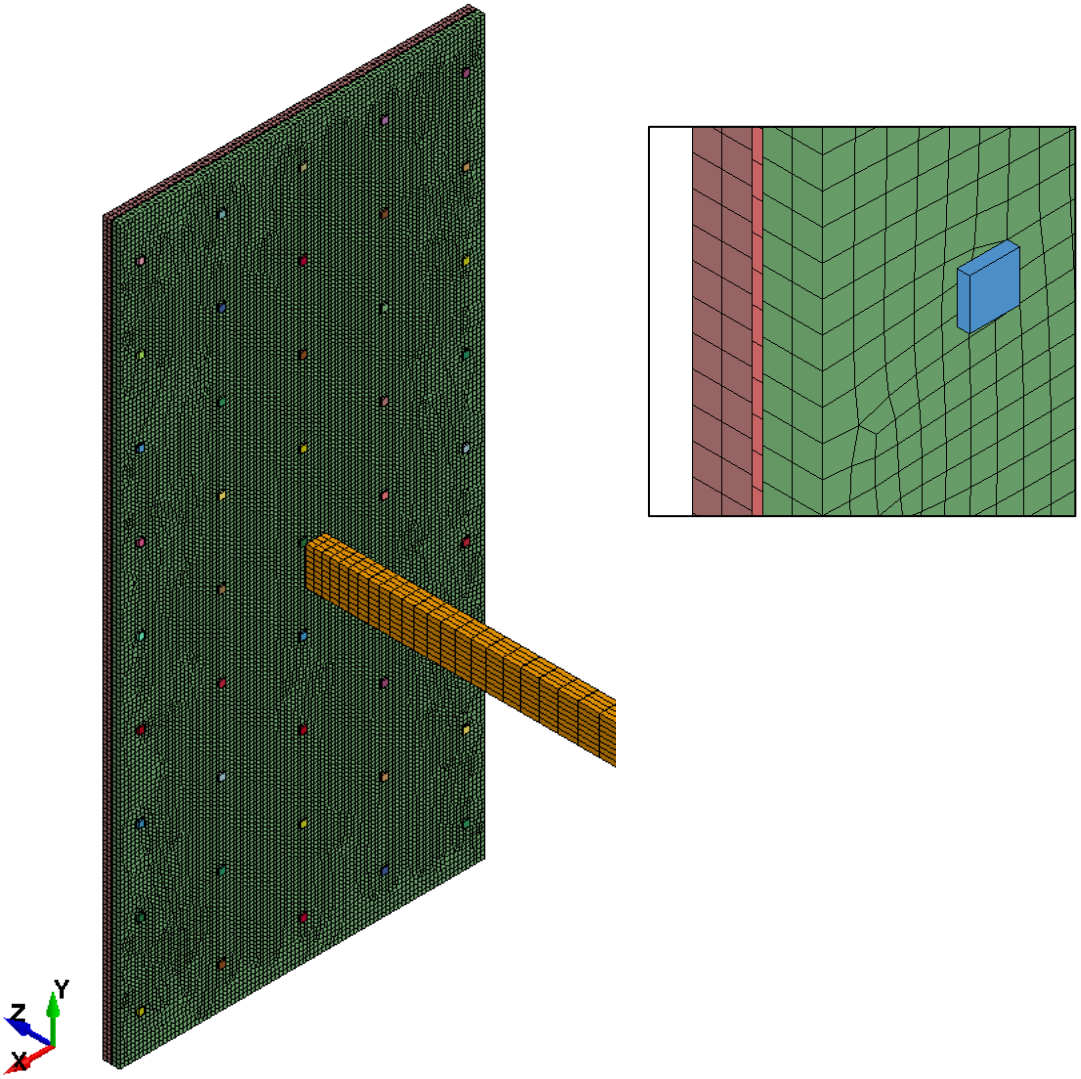

Figure 4.1.1 - Door model geometry showing mesh. The detail in the upper right corner of the figure shows the relative sizes of the wood, steel, and bolt elements. A refined mesh with multi-zone mapping was implemented for maximum accuracy.

RESULTS

As expected, the door withstood the impact with little damage and no evidence of perforation. The maximum deformation of the door was around 13 mm or 0.51”. Unlike previous impacts into solid materials, the door was allowed to flex and bend as an elastic plate. Thus, the door deflected more significantly under impact. Because of the high acceleration levels in the case of an impact, it is not recommended for occupants to be in contact with the door.

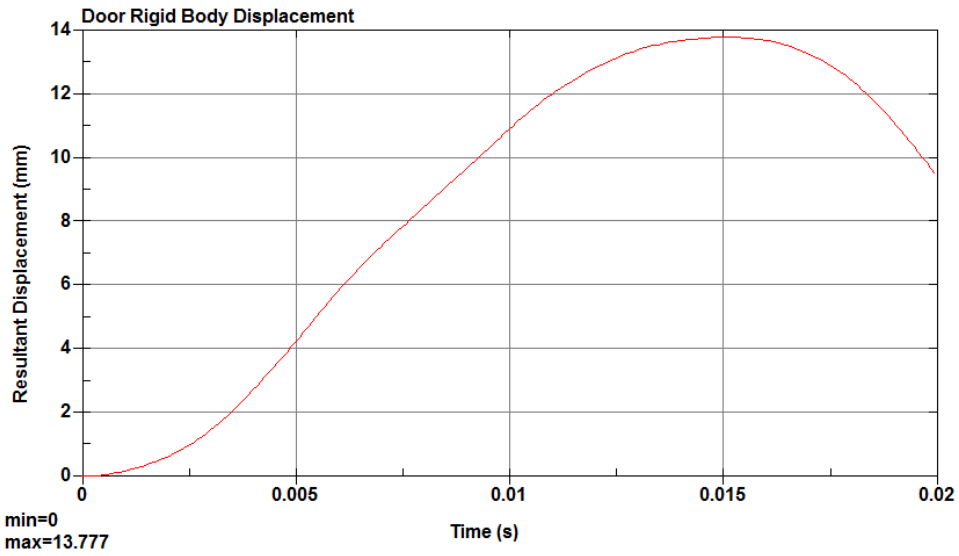

Figure 4.1.2 – Rigid body displacement of the door.

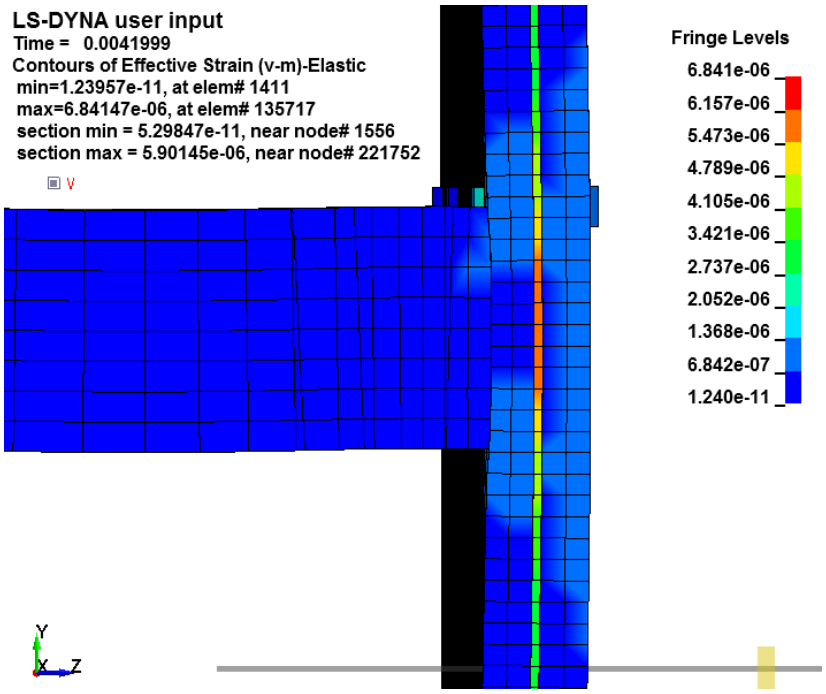

Figure 4.1.3 -Test 4.1 detail showing discontinuous strain through the door. Fringe levels show v-m strains in mm/mm.

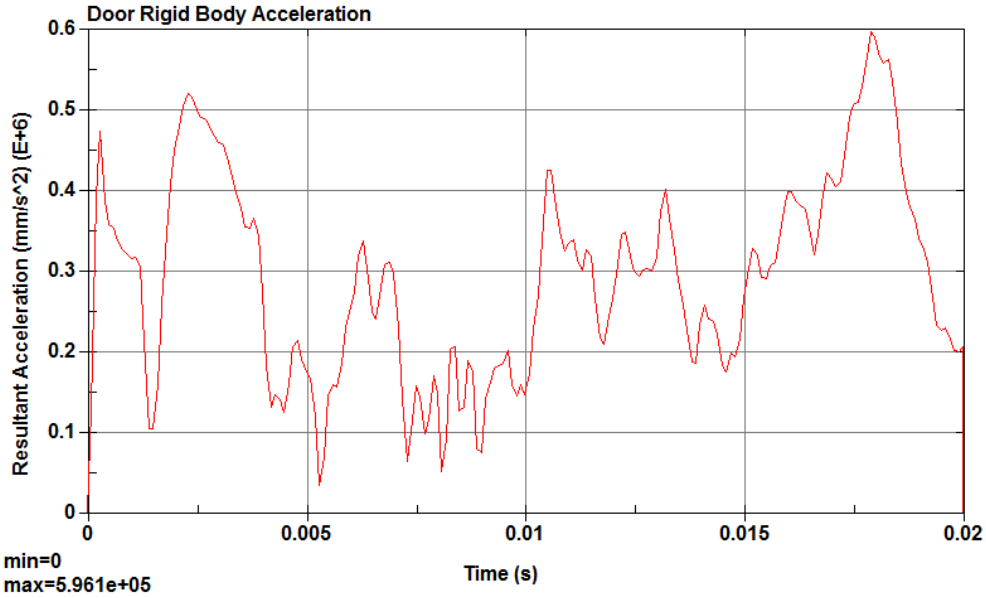

Figure 4.1.4 –Acceleration plot for the door assembly in simulation 4.1.

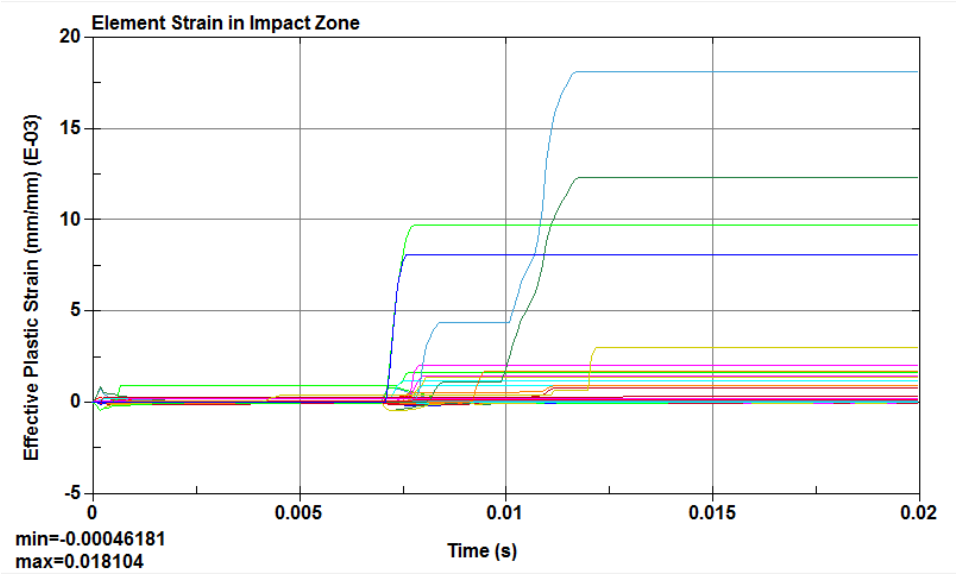

Figure 4.1.5 - Select element strains for simulation 4.1. The lines represent a sample of elements throughout the thickness of the door.

SECTION 5: VEHICLE IMPACT

In addition to projectiles with low relative elastic moduli and hard, rigid projectiles, some projectiles consist of thin-walled rigid materials. The materials in these projectiles can be denser than concrete, but the projectile will still be highly deformable under impact. Cars are an example of such projectiles; they are both commonplace and likely to be abandoned during an approaching tornado. As such, the impact on a saferoom from a car must be considered in its design.

The goal in the following simulations was to understand how a car behaves as a projectile, how a saferoom withstands the impact from a falling or rolling car, and how the damage from such an impact can be characterized.

Although many potential impact scenarios were possible, the research team limited the scope of the initial study to head-on collisions at the center of the wall or ceiling slab. The rationale was that the center of the slab was most prone to deformation and spalling, and was therefore the weakest point. A head-on collision was selected because it would result in the most complete energy transfer into the saferoom. A glancing collision, although having less surface area, results in significant energy loss via scraping. Any damage from such collisions is cosmetic, and would not pose a threat to structural integrity of the saferoom.

VEHICLE MODEL (5.0)

A Chevrolet C2500 Pickup finite element model was chosen for the vehicle crash tests. This model was developed by the National Crash Analysis Center (NCAC) under a contract with the Federal High Way Administration of the US DOT. The reduced model, shown in Figure 5.0.1, has 10,500 elements and was used for initial tests to save computational time. The detailed model, with 58,313 elements, was used for the full-scale tests.

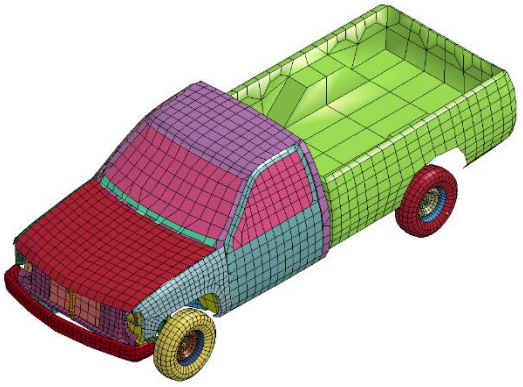

Figure 5.0.1- C2500 FE reduced model. This model does not include seats or airbags like the detailed model, but preserves the mass and weight distribution of a pickup truck.

Before running any impact simulations with the concrete, the vehicle model was tested on a rigid wall to ensure stable model performance. It was found that under optimal conditions, a 150 ms rigid wall crash simulation completed in approximately 100 minutes. The machine specifications included an 8-core processor at 3.5 GHz and 16 GB of allocated RAM.

Some modifications were made to the vehicle model to improve runtime performance. The element contact formulation was changed to soft (TYPE 1) to improve the bumper-concrete interface. An initial velocity was applied to all nodes to simulate wind-driven coasting. The radiator element section was reformulated to the standard form (ELFORM 1) in order to avoid negative volume errors. These modifications eliminated certain behaviors of the vehicle model that help assess the damage done to the car. The focus of this study, however, was the effect of a vehicle crash on a concrete barrier, and the small internal inaccuracies of the vehicle model were neglected.

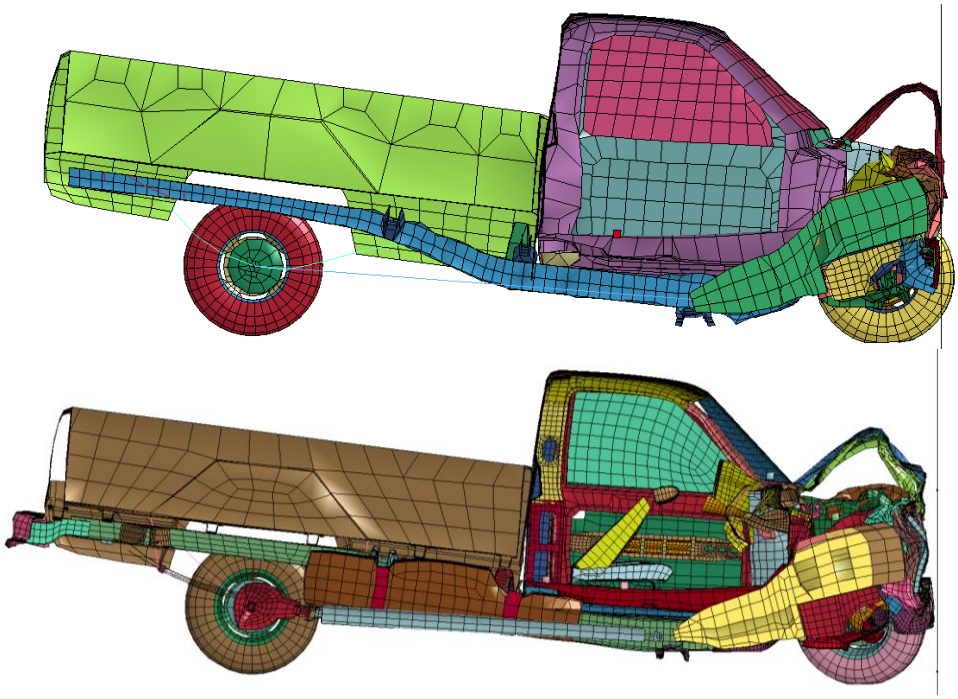

Figure 5.0.3 - A cross-section comparison of the reduced and detailed vehicle models colliding into a rigid wall at 35 mph. Note the engine block and transmission being pushed upwards and forward into the wall as the front of the car crumples. Future simulations are shown with the vehicle omitted in order to give a better view of the damage patterns on the concrete slab.

IMPACT SIMULATION SETUP

In all component simulations, a vehicle with an initial velocity impacted a thick reinforced wall fixed at the sides. One notable distinction from a vehicle crash test is that rather than the velocity and acceleration applied solely to the wheels of the vehicle, an initial velocity was applied to all nodes with no acceleration. This more accurately simulates a coasting vehicle being pushed by tornado winds. The model was put together in LS-PrePost and had some 350,000 elements, most of which were solid elements in the concrete slab. Various simulation parameters are shown above in Table 5.0.1. A total of ten scenarios were analyzed, as shown in Table 5.0.2.

Table 5.0.1 - Table of simulation parameters. Sources of the parameters were either specified by the sponsor (OZ Saferooms) or adapted from NCAC models and common practices.

Group	Name	Value	Unit	Source	Notes
Slab	Width (Y)	3302	mm	OZ	eqv. 130"
Slab	Height (Z)	3302	mm	OZ	eqv. 130"
Slab	Thick. 1 (X)	457.2	mm	OZ	eqv. 18"
Slab	Thick. 2 (X)	203.2	mm	OZ	eqv. 8”
Slab	Rebar	#4	Gauge	OZ	eqv. 0.5" OD
Projectile	Mass	1923	kg	NCAC	eqv. 4,250 lb
Projectile	Initial Vel. 1	11176	mm/s	OZ	eqv. 25 mph
Projectile	Initial Vel. 2	15646	mm/s	NCAC	eqv. 35 mph
Simulation	No. Elements	356313	-	none	for roof slab
Simulation	Runtime	1:50	h:m	none	Approximate

Table 5.0.2 - Table of simulation runs. The tests are referred to by their number and name interchangeably. The numbers at the end of the file name indicate the impact velocity, the letters are short for Detailed (D), Detailed-Side (DS) and Detailed-Roof (DR).

Test No.	Test Name	Date Run	Description	Comments
5.0	TestCrash35	7/23/2015	Rigid wall impact	Test for runtime stability
5.1	RoofCrash25	7/23/2015	18-inch roof @ 25 mph	Withstood impact
5.2	RoofCrash35	7/24/2015	18-inch roof @ 35 mph	24" hemisphere damage zone
5.3	SideCrash25	7/28/2015	8-inch wall @ 25 mph	Small damage
5.4	SideCrash35	7/29/2015	8-inch wall @ 35 mph	Possible spalling, plug formation
5.5	SideCrash35D	8/05/2015	Test 5.4 with detailed car	No plug, risk of spalling
5.6	FullCrash35DS	8/10/2015	Full saferoom @ 35 mph	Side crash, no plug
5.7	FullCrash35DR	8/14/2015	Full saferoom @ 35 mph	Roof crash, tilted car, low damage
5.8	FrontCrash35D	8/24/2015	Full saferoom @ 35 mph	Crash into door opening
5.9	FrontCrash35DS	8/26/2015	Full saferoom @ 35 mph	Crash into door opening, sideways

ROOF IMPACT

25-MPH IMPACT (5.1)

The first simulation to be evaluated was the safest scenario – a 25 mph free-fall onto the roof of the OZ saferoom. The test, shown in figure 5.1.2, completed efficiently and was post-processed to selectively obtain simulation data about the concrete response. A few high-level metrics were used evaluate the performance of the protective enclosure. As in the literature dealing with concrete impacts, depth of penetration is a crucial measure. This metric is supplemented with back-wall displacement and resultant acceleration. The time history for a node in the impact area is shown in Fig. 5.1.2 and wall rigid body acceleration in Fig. 5.1.3.

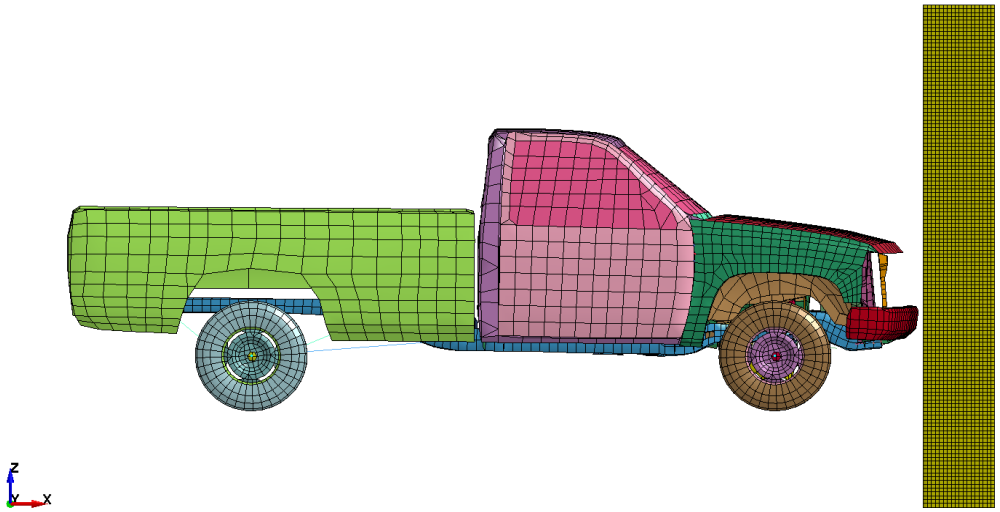

Figure 5.1.1 – RoofCrash model showing the truck and slab with reinforcement. Gravity is in the positive x-direction. The setup is identical to wall crash tests, except for slab dimensions and initial velocity.

Table 5.1.1 - Simulation metrics for RoofCrash25 and RoofCrash35 tests.

Metric	Units	RC25	RC35
Max. Displacement	mm	0.05	0.87
Max. Acceleration	m/s^2	9.96	150
Max. Plastic Strain	mm/mm	0.27	1.92
Damage area	cm^2	125	2919
Damage Depth	mm	20	304.8

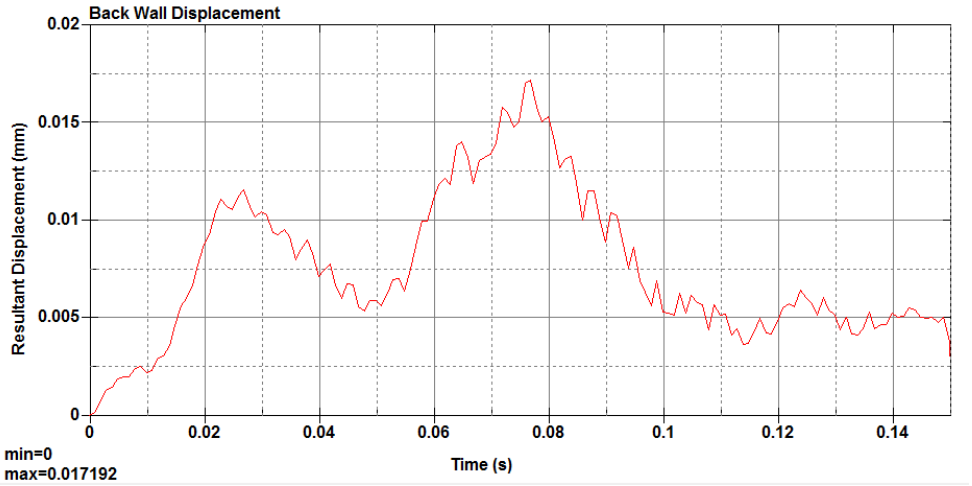

Figure 5.1.2 - Concrete Wall displacement for the RoofCrash25 simulation. Note a maximum strain rate of 1.2 mm/s. High-frequency noise was filtered out by a moving 5-point average.

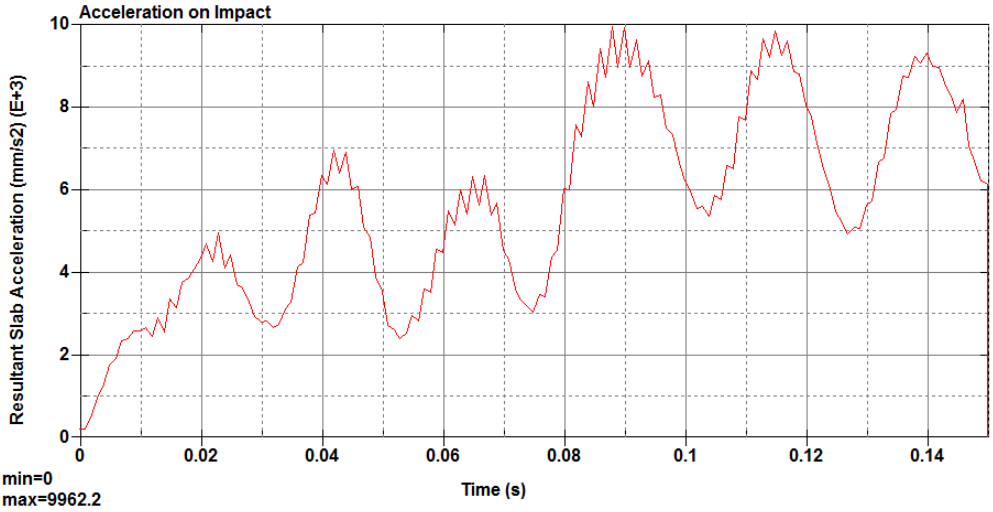

Figure 5.1.3 - Concrete roof acceleration for the RoofCrash25 Simulation. High-frequency noise was filtered out by a moving 5-point average filter.

In addition to the quantitative results, the damage tracking variable in RHT concrete is displayed, and analyzed qualitatively. The damage fringes are compared to the plastic strain fringes for further validation and assessment of qualitative effects such as spalling. Accumulated damage zones are shown in Figure 5.1.3. Numerical data is also summarized in Table 5.1.1 for ease of reference.

The simulation shows an extremely low overall displacement: 0.017 mm at the maximum (Figure 5.1.2). The concrete slab hardly deforms, and the concrete in the back experiences low strain rates, as shown by the slope of the displacement curve, which has no discontinuous singularities. The acceleration, too, is within the range of 5-10 m/s^2, corresponding to the sandbag experiment found by RIT Senior Design Team in 2012. Thus, the data imply that a 25 mph impact into the roof is completely safe, with no expected fracture, internal damage or spalling.

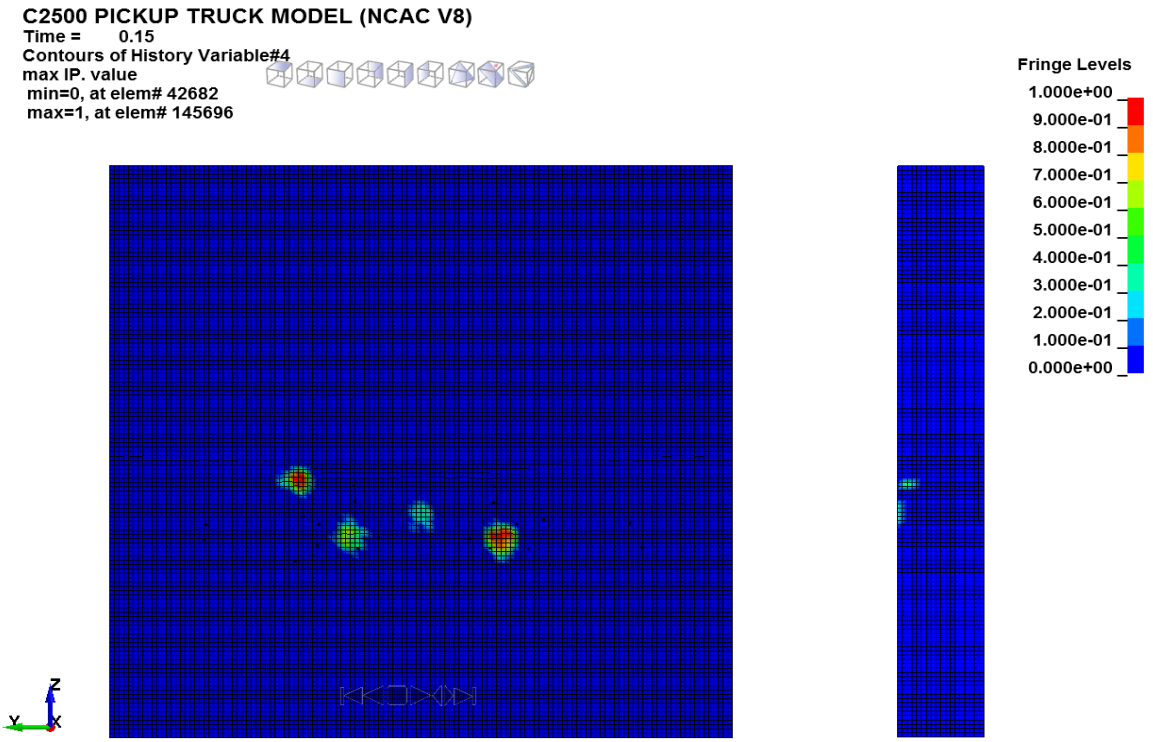

Figure 5.1.3 - Damage accumulation at the end of the RoofCrash25 impact. Front and cross-section views.

This is confirmed by the damage patterns in Figure 5.1.3. All severe damage is limited to the surface of the concrete, and occurs at sharp edges of the vehicle model such as the hood and fender brackets. Plastic strain is low, indicating that sustained damage did not result in extended deformations.

35-MPH IMPACT (5.2)

The 35 mph impact differs lonlinearly from the previous simulation. The engine brackets that were able to prevent the detachment of the engine in the 25 mph test fail in the 35 mph test. As a result, the engine block itself impacts the roof, resulting in a hard impact scenario.

The displacement and acceleration plots (Figs. 5.2.1 and 5.2.2) show that, starting at 40 ms, the slab experiences a large impulse, resulting in an acceleration spike two orders of magnitude higher than the 25 mph test. The resulting residual strain is quite significant, though the maximum displacement is not so high as to cause physical damage to occupants of the saferoom.

Metric	Units	RC25	RC35
Max. Displacement	mm	0.05	0.87
Max. Acceleration	m/s^2	9.96	150
Max. Plastic Strain	mm/mm	0.27	1.92
Damage area	cm^2	125	2919
Damage Depth	mm	20	304.8

Table 5.1.1 reproduced for the reader's convenience.

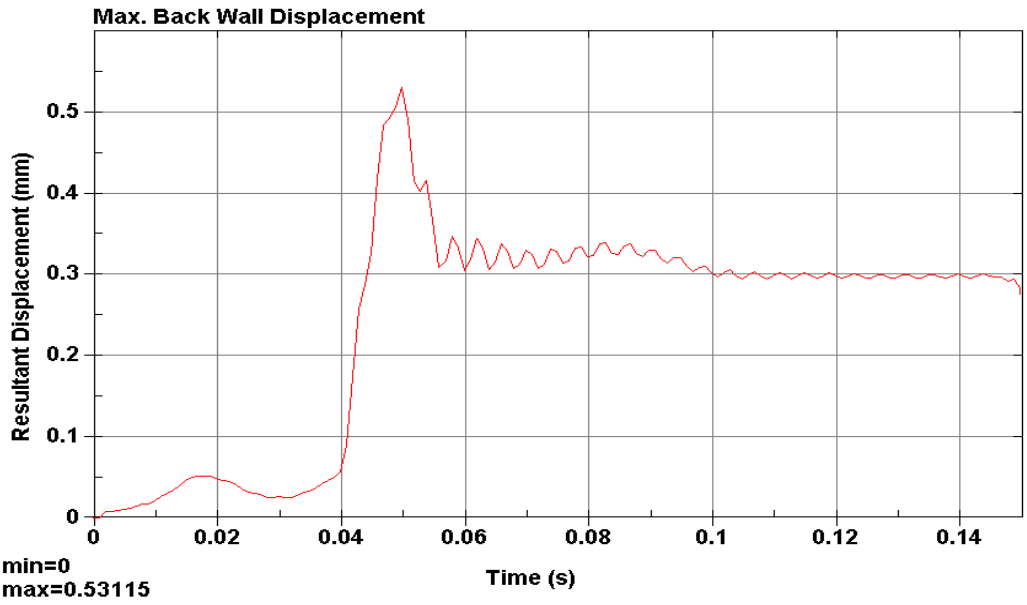

Figure 5.2.1 - Concrete Wall displacement for the RoofCrash35 simulation. Note the very high strain rate at 40 ms, corresponding to the transition from soft to hard impact. High-frequency noise was attenuated.

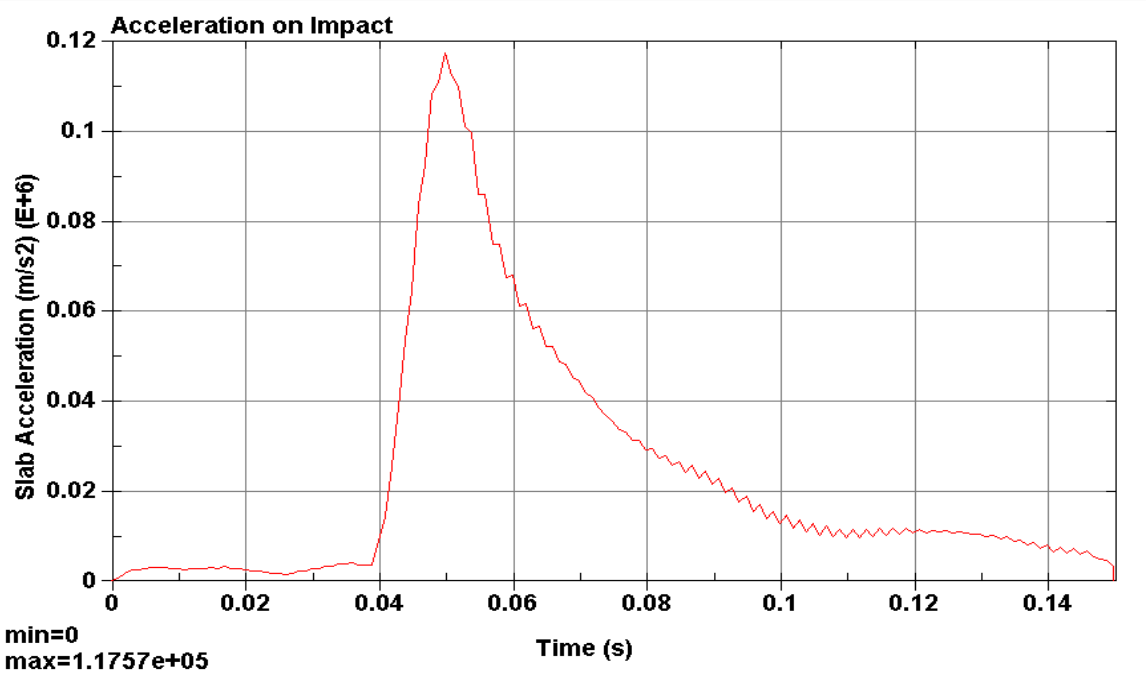

Figure 5.2.2 - Concrete roof acceleration for the RoofCrash35 Simulation. High-frequency noise was attenuated.

The damage pattern and plastic strain visualization also shows significantly different results. A large "damage crater" is formed after the impact with the engine, stopping short of the rebar layer, and not reaching the back wall. Although this damage zone does not necessarily correspond to penetration, it does indicate that the concrete compressive strength has been exceeded, and that from a safety perspective the concrete should be considered eroded[1]. Additionally, some slight damage on the inside wall may be an indicator of possible spalling.

At first glance, it is unclear whether these results should be considered valid, as the magnitude of deformation was unexpected. Nevertheless, this test is included to show chronological progression of work conducted.

[1] Concrete that has reached maximum damage is assumed to have lost all its shear and tensile strength, therefore making it susceptible to rapid weathering and deterioration under thermal or mechanical cycling.

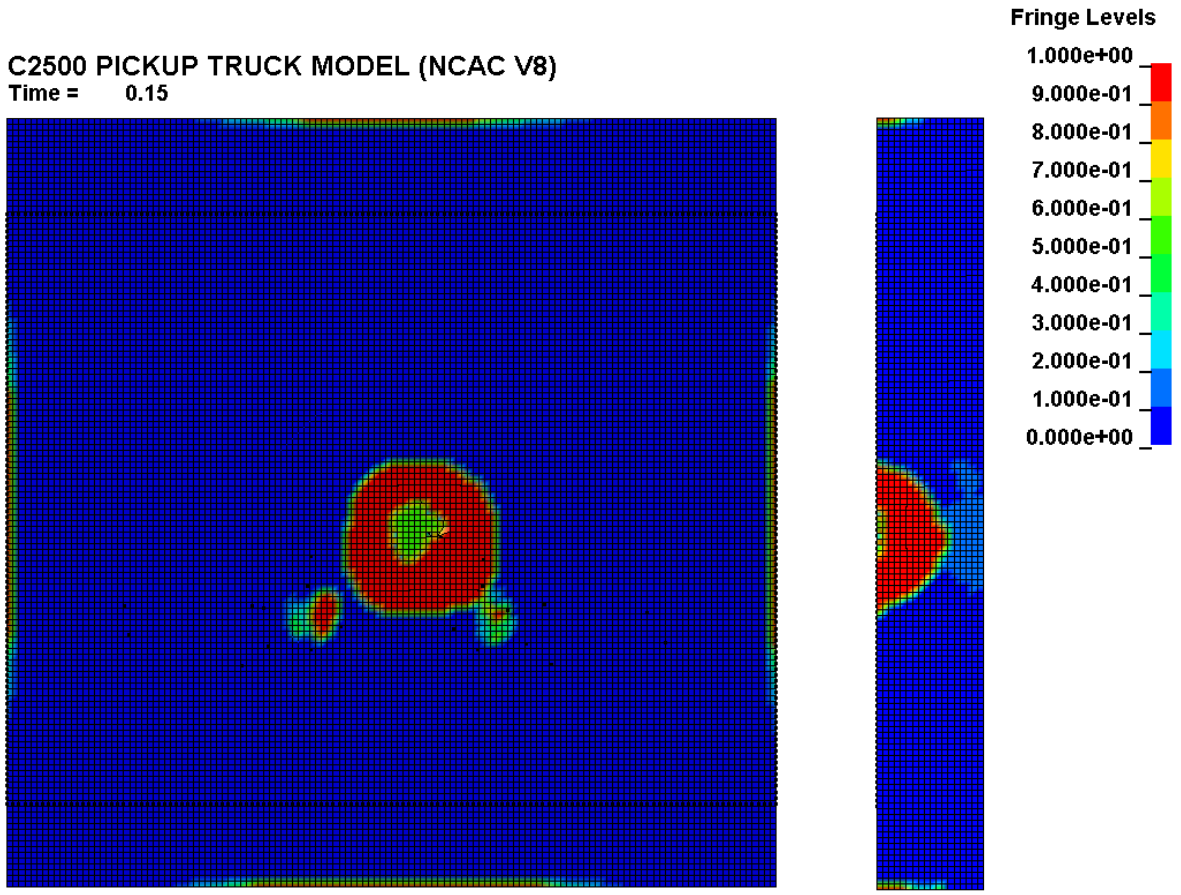

Figure 5.2.3 - Damage accumulation at the end of the RoofCrash35 impact. Front and cross-section views.

ANALYSIS

Overall, the roof is able to absorb the impact without catastrophic failure, although spalling is a possible threat if the concrete is pre-damaged. Special consideration was given to the validation of the soft-hard transition, as the damage caused was not in agreement with the NDRC formula. Possible sources of inaccuracy are specific element interactions in the vehicle model, or possibly the fixed constraints at the side faces of the roof. Therefore, changing the boundary conditions or the detail level of the vehicle model would either validate or disprove the results of the current test. Tests 5.5 and 5.7, respectively, implement these modifications.

SIDE-WALL IMPACT

25-MPH IMPACT (5.3)

In addition to a simulated vehicle drop, a vehicle crash into the side wall was studied. The side wall analyses have two differences from the roof model: the wall is slender and higher, having an 8-inch thickness, and the gravity is now applied in the negative Z-direction. As in simulation 5.1, the 25 mph impact causes insignificant damage. The maximum deflection is less than a millimeter, and the damaged area is comparatively small: 244 cm^2. Two peaks can be seen in the displacement and acceleration plots in figures 5.3.1 and 5.3.2. The times correspond to the chassis rails and the engine support rails contacting the concrete slab, respectively.

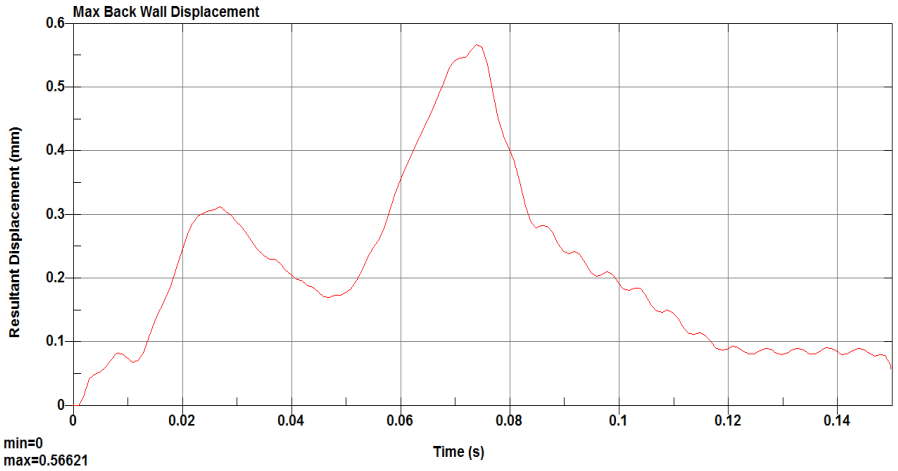

Figure 5.3.1 - Concrete wall displacement for the SideCrash25 simulation. High-frequency noise was attenuated.

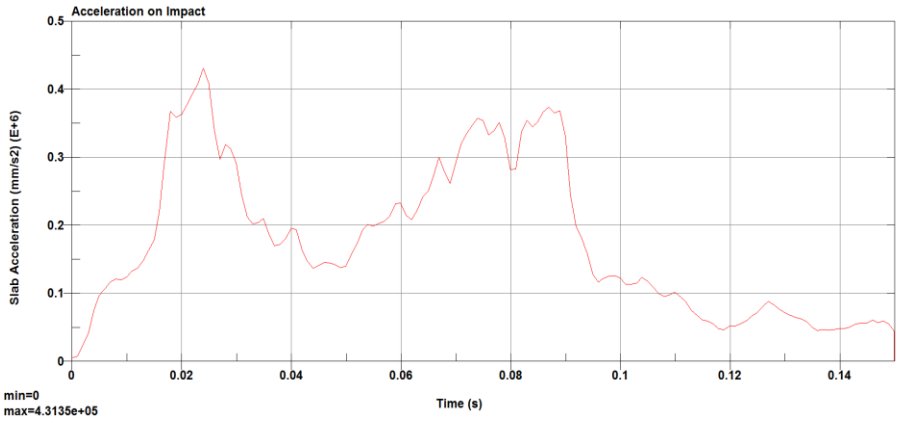

Figure 5.3.2 - Concrete wall acceleration for the SideCrash25 simulation. High-frequency noise was attenuated.

The penetration pattern in the 25 mph side impact, Figure 5.3.3, closely resembles the 25 mph roof impact. Two symmetrical damage zones form at the location of the main chassis rails, with some slight additional damage from the hood, fender, and bumper. The bulk of the energy is dissipated in deformation of the engine support and rail, but the engine block does not contact the wall.

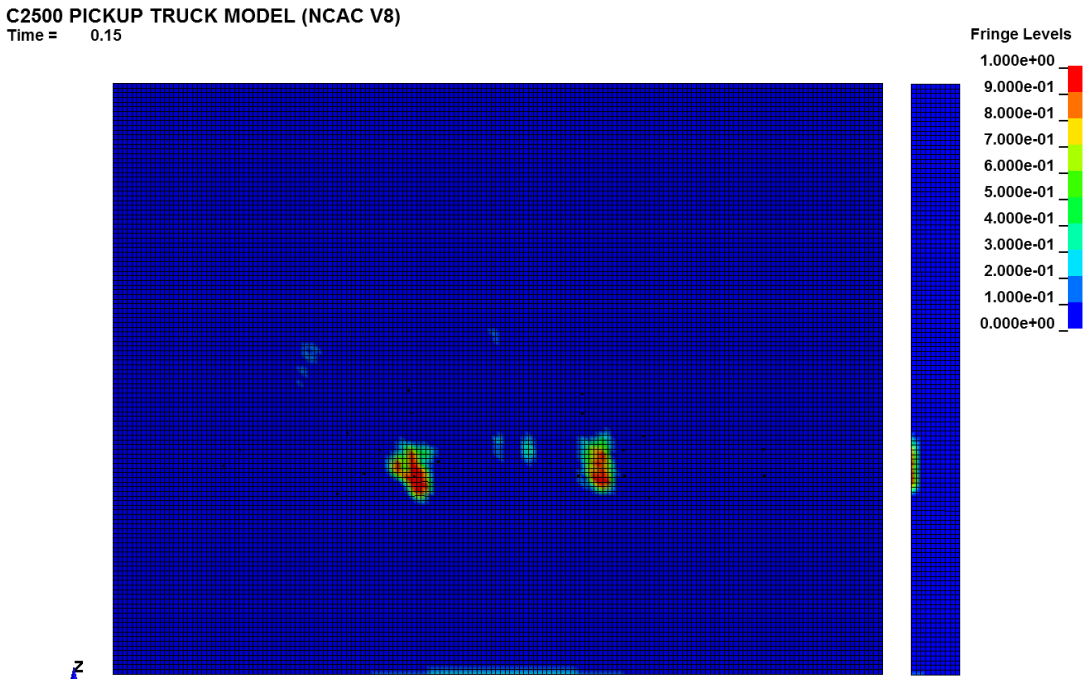

Figure 5.3.3. - Damage accumulation at the end of the SideCrash25 impact. Front and cross-section views. Note the symmetrical damage zones in the lower half of the slab. These are from the initial contact of the chassis frame with the slab, and will reappear frequently for this model of vehicle.

35-MPH IMPACT (5.4)

Following the success of the 25-mph crash test, the 35-mph test was run. It was expected that the wall would fail, due to the 12-inch damage depth observed in test 5.2. Still, the results, Figures 5.4.1 and Figure 5.4.2, were post processed to obtain comparative data.

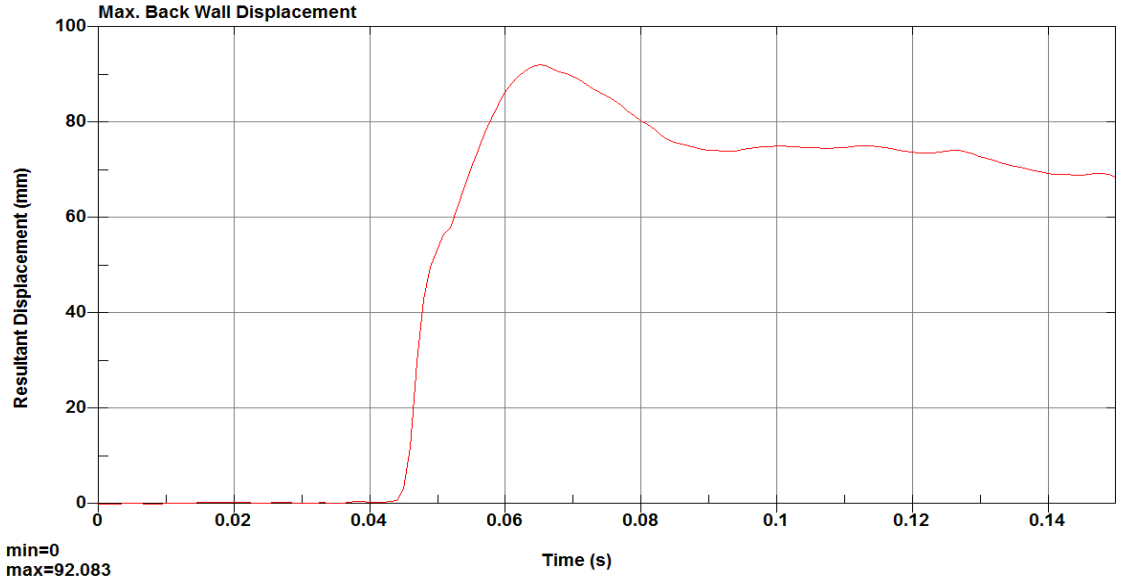

Figure 5.4.1 - Back wall displacement for SideCrash35 simulation. Notice the rapid increase in displacement occuring at 45 ms. This corresponds to the engine block in the vehicle contacting the concrete slab.

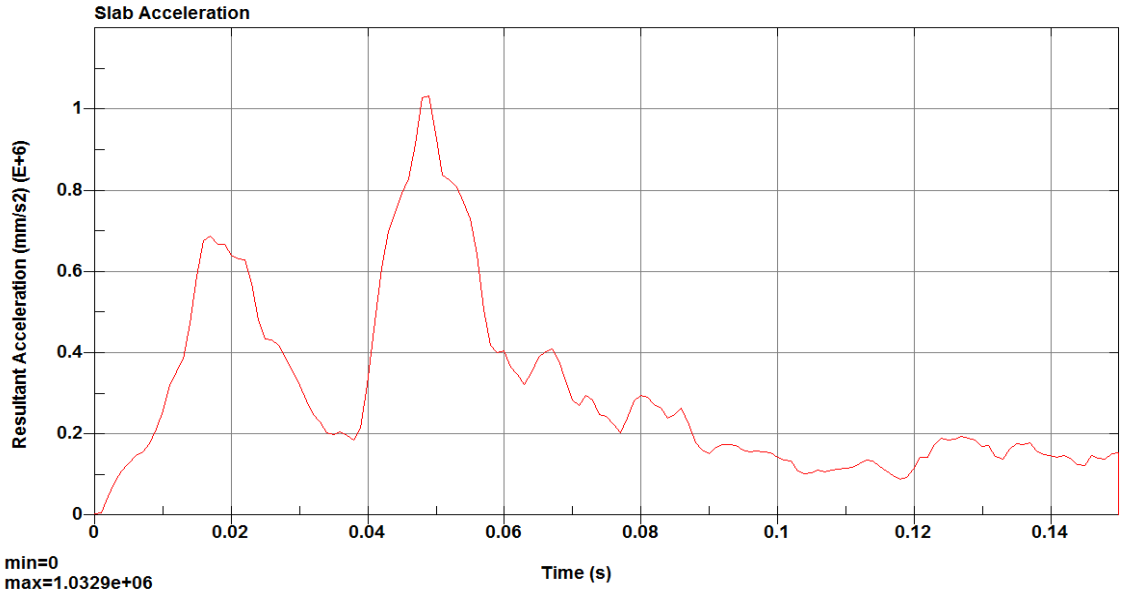

Figure 5.4.2 - Resultant acceleration for SideCrash35 simulation. Data filtering applied to attenuate high-frequency noise. Note two clear impulse peaks, corresponding contact from the chassis frame and the engine block, respectively.

There is a huge difference between the results of the 25 and 35 mph side crashes. This is because in the 35 mph impact, the engine block in the vehicle makes direct contact with the concrete wall, causing extremely rapid damage formulation (refer to animation SC35_H4_Xsec.avi). Additionally, the concrete forms a plug, as seen in Figure 5.4.3 (side view), implying catastrophic damage as well as penetration of debris into the interior of the saferoom.

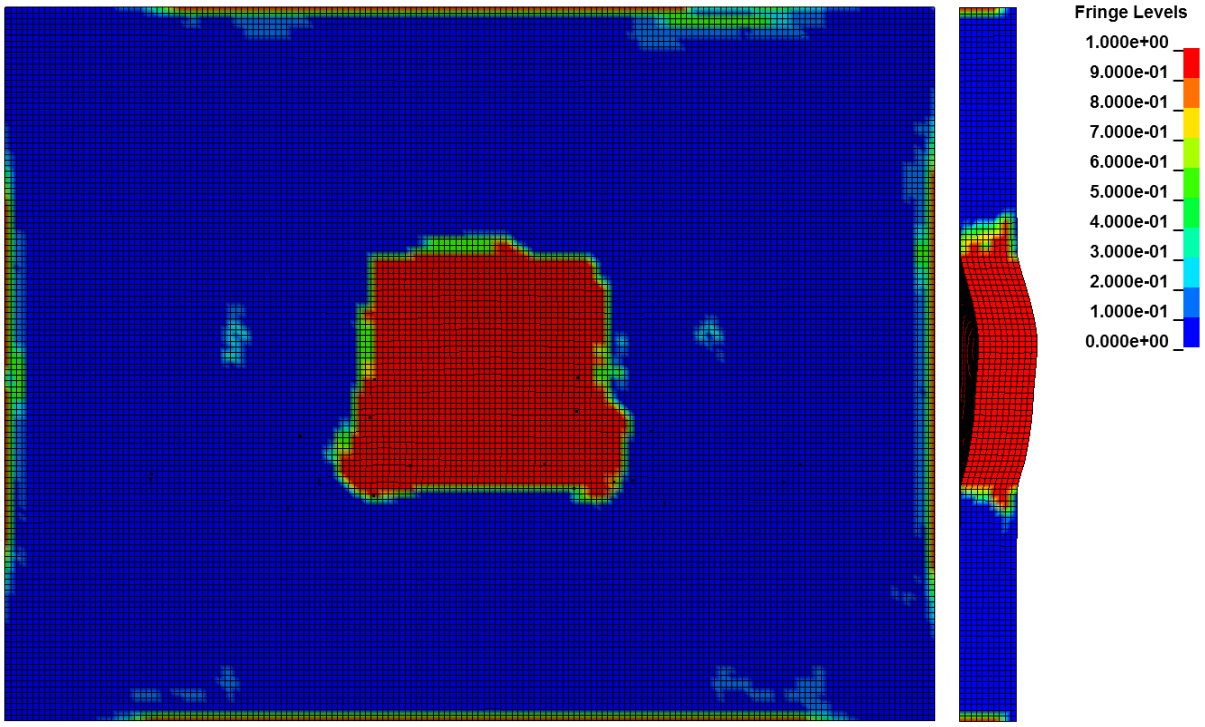

Figure 5.4.3 - Damage accumulation pattern in SideCrash35. Full plug formation and penetration occurs in the center of the wall. The failure region is limited by the rebar geometry, giving a roughly square damage zone measuring 800 mm to a side.

Naturally, these results directly imply that the saferoom cannot withstand a 35 mph crash. However, the results and figures must be understood in more detail before broad conclusions are drawn. In the case of catastrophic failure, element energies can often reach disproportionately high values, giving arbitrary results. In the case of this simulation, the accelerations for the concrete slab was ten times higher than expected. Thus, the quantitative results of simulation 5.4 cannot be accepted as accurate without further validation.

DETAILED 35-MPH IMPACT (5.5)

Among all simulations run, the side wall impact featured the highest impact velocity along with the thinnest wall. The measured penetration from test 5.4, however, was an order of magnitude larger than the NDRC formula prediction for a hard impact of equivalent mass. Thus, the slab and vehicle model were both refined to provide more detailed results, in hopes of dispelling this discrepancy.

The vehicle mesh dependency was checked in this scenario, and the detailed vehicle model (See 5.0) was implemented in place of the reduced model. A mesh convergence study was also applied in the concrete wall. For both cases, computational time, hourglass energy, and mass scaling were considered. The final simulation configuration had 265,000 elements and the test completed in approximately 12 hours. Tests results for side crashes are tabulated in Table 5.5.1. Figure 5.5.1 shows a maximum displacement compatible with the NDRC formula, the acceleration level seen in Figure 5.5.2. Figure 5.5.3 shows the accumulated damage patterns. Even with smaller displacement and acceleration, there is a risk of spalling.

Table 5.5.1 - Simulation metrics for side Crash tests 25, 35, and 35D.

Metric	Units	SC25	SC35	SC35D
Max. Displacement	mm	0.556	92.1	2.85
Max. Acceleration	m/s^2	431	1033	28.77
Max. Plastic Strain	mm/mm	0.122	1.45	0.4047
Damage area	cm^2	240	6400	244
Damage Depth	mm	20	202	202

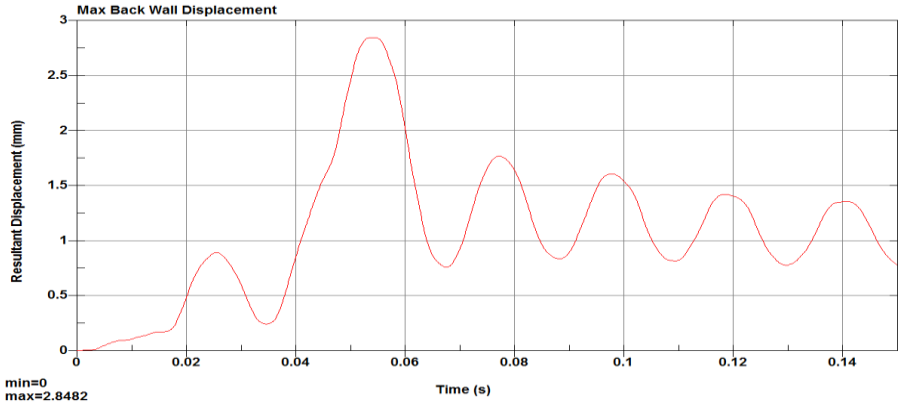

Figure 5.5.1 - Back wall displacement for SideCrash35D simulation. The displacement is much less than the reduced model, and the characterisitic damped modal response of a reinfoced slab can be seen here (refer to initial rebar tests).

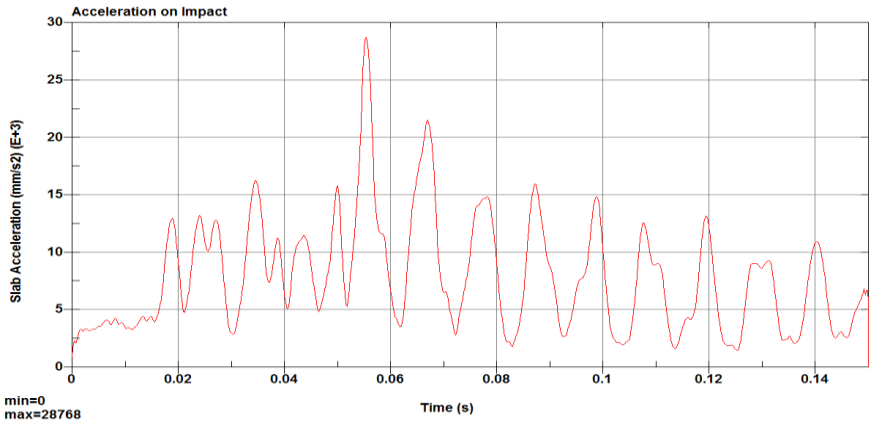

Figure 5.5.2 - Resultant acceleration for SideCrash35D simulation. Data filtering applied to attenuate high-frequency noise.

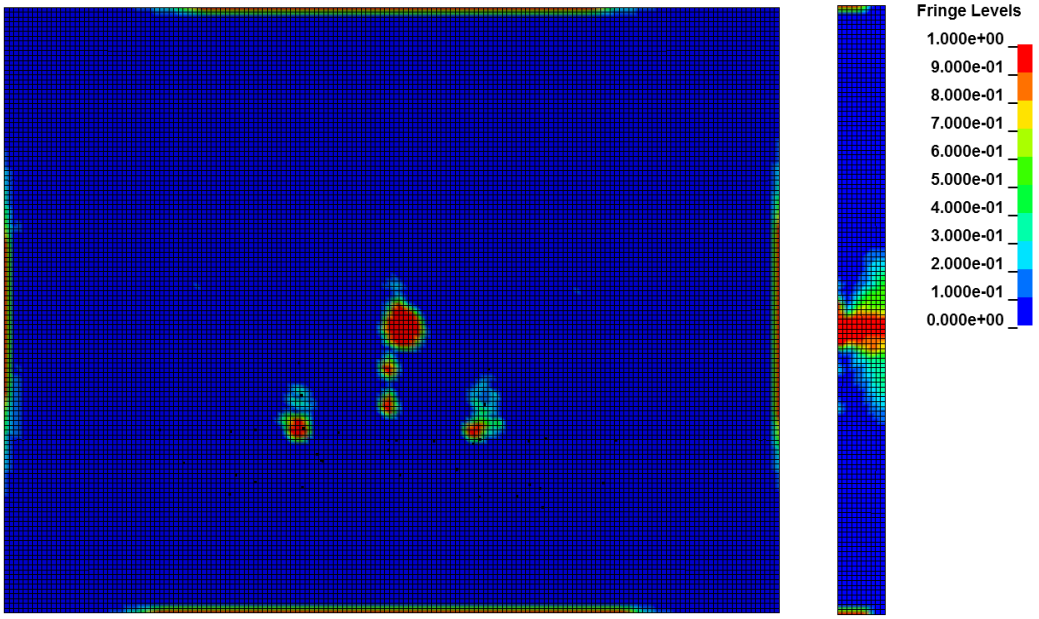

Figure 5.5.3 – Damage accumulation pattern for the SideCrash35D. Front and cross-section views. Although the impact zone from the engine block is also visible, the damage from it is much more consistent with theoretical predictions.

ANALYSIS

The Side crash tests were able to confirm the ability of the saferoom to withstand all impact scenarios with the vehicle. Figure 5.5.4 shows a velocity plot of a range of points in the front, middle, and back of the vehicle. Much of the velocity was absorbed uniformly, with some parts, such as the tires and engine, experiencing a slight lag in the time of their deceleration.

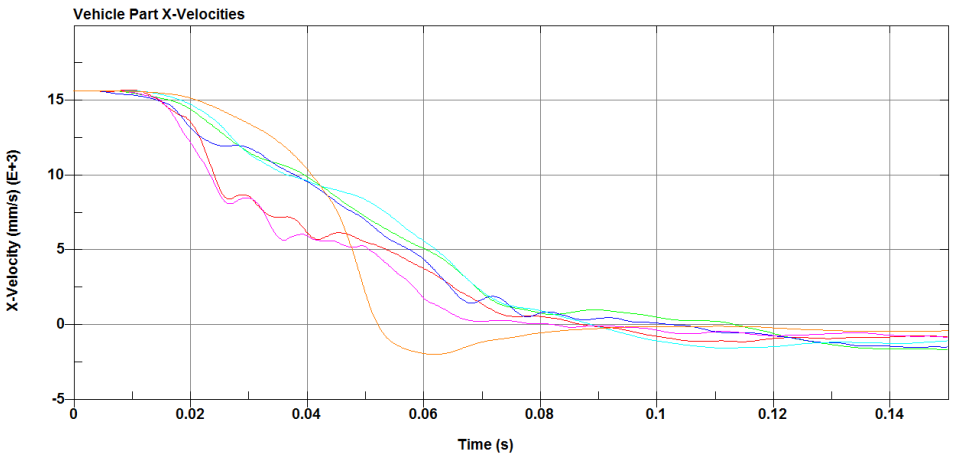

Figure 5.5.4 - X-Velocities at various points in the vehicle. Velocities below zero indicate that the vehicle rebounds from the wall.

Not all scenarios, however, were able to protect the occupants from possible spalling. Test 5.5 confirmed that damage to the back wall was possible for crashes exceeding 35 mph. The authors will recommend considering this limitation when developing design constraints for the saferoom.

FULL-SCALE MODEL

After the completion of preliminary and component tests, a full scale model could be assembled with some confidence in the accuracy and runtime. The model, Figure 5.6.0, has about 360,000 elements, with 60,000 elements in the vehicle, 200,000 elements in the refined impact zone, and 100,000 elements for the remaining wall, roof, and soil geometry. The full-scale saferoom is mounted in soil, and is not directly constrained. Instead, impact and pressure loading will be applied to the walls, which will transfer the load into the soil. This allows for a variety of possible impact scenarios, such as debris impacts, vehicle impacts and collapsing-structure impacts.

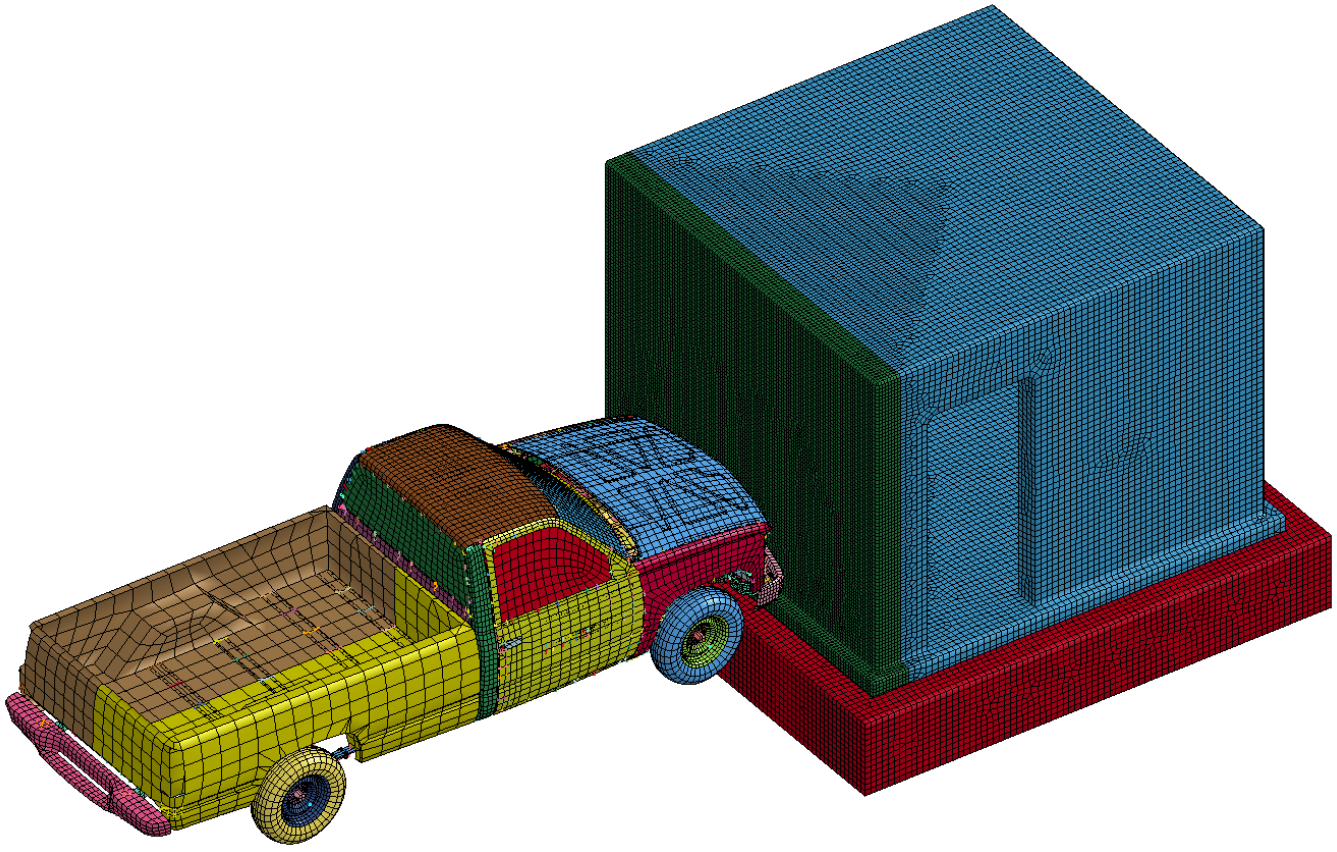

Figure 5.6.0 – Input file for FullCrash35DS simulation. The refined wall is shown in green, the coarse-mesh shelter is shown in blue, and the soil in red. Boundary conditions are applied to the soil only – therefore the full dynamic response of the saferoom can be seen.

35-MPH SIDE IMPACT (5.6)

The side impact was carried out to address the concerns discussed in test 5.5 in more detail. Figure 5.6.1 shows the maximum displacement in the intern face of the sidewall. It is similar to Figure 5.5.1 regarding the two peaks at 0.025s and 0.055s, although the peaks are not as distinct. Furthermore, the maximum displacement is 42% lower than in the single wall model, mainly because the vehicle hits the wall at the ground level instead of impacting in its center.

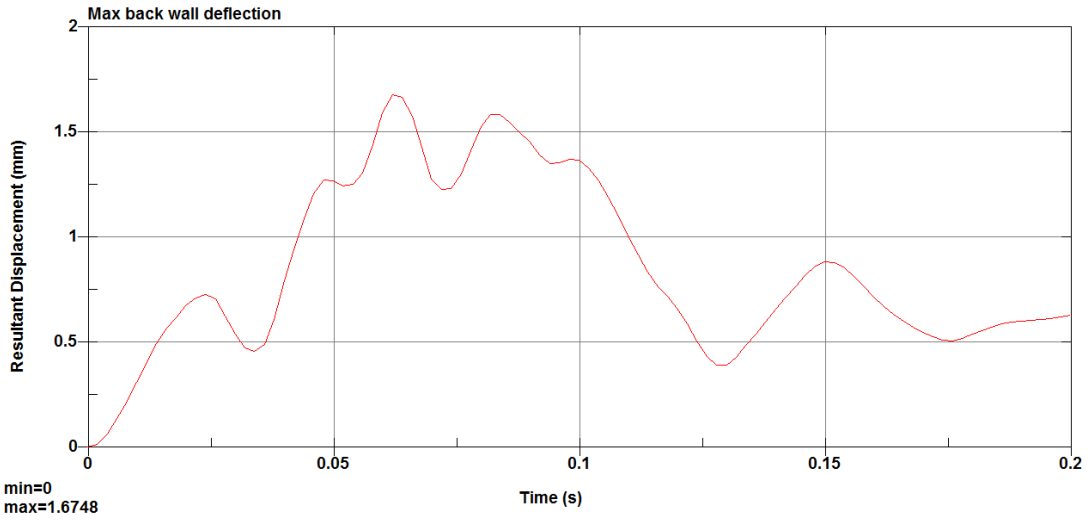

Figure 5.6.1 - Back wall displacement for FullCrash35DS simulation. The superposition of modal response of the sidewall and other vibration modes of the saferoom can be seen here.

The wall's modal response differs due to the change in boundary conditions and the added mass of the rest of the saferoom. The removal of fixed constraints cause a decrease in the acceleration level in the sidewall as seen in Figure 5.6.2. The non-zero initial acceleration is caused by the initial penetration of the sectioned sidewall into the remainder of the shelter.

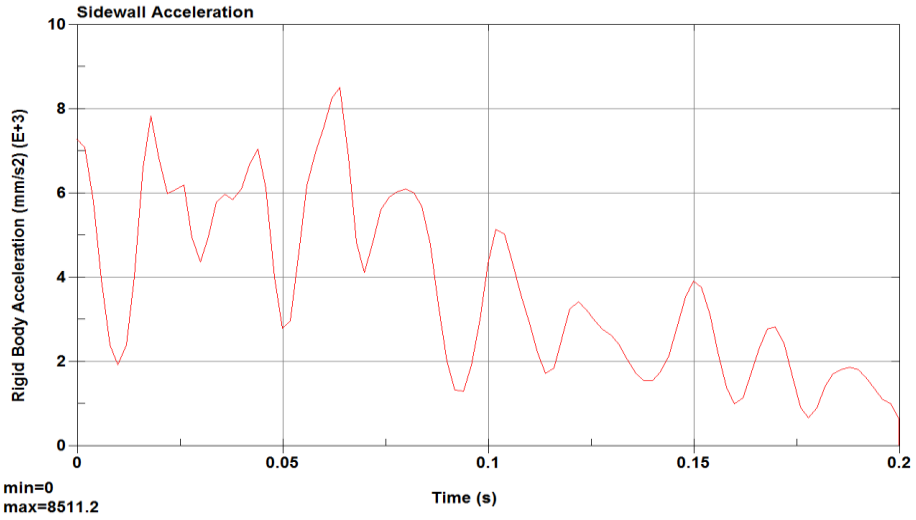

Figure 5.6.2 - Resultant acceleration for FullCrash35DS simulation. Two point data filtering applied to attenuate high-frequency noise.

The damage is shown in Figure 5.6.3 is most evident near the ventilation holes and in the floor corner where there is stress concentration. It can be seen that the decrease in impact height and removal of fixed constraints in the wall are effective to reduce damage. Additionally, some incidental damage can be seen in the top left and bottom right corners. This damage is due to the way the detailed wall is bonded onto the rest of the saferoom geometry, and will not cause failure in the monolithic structure.

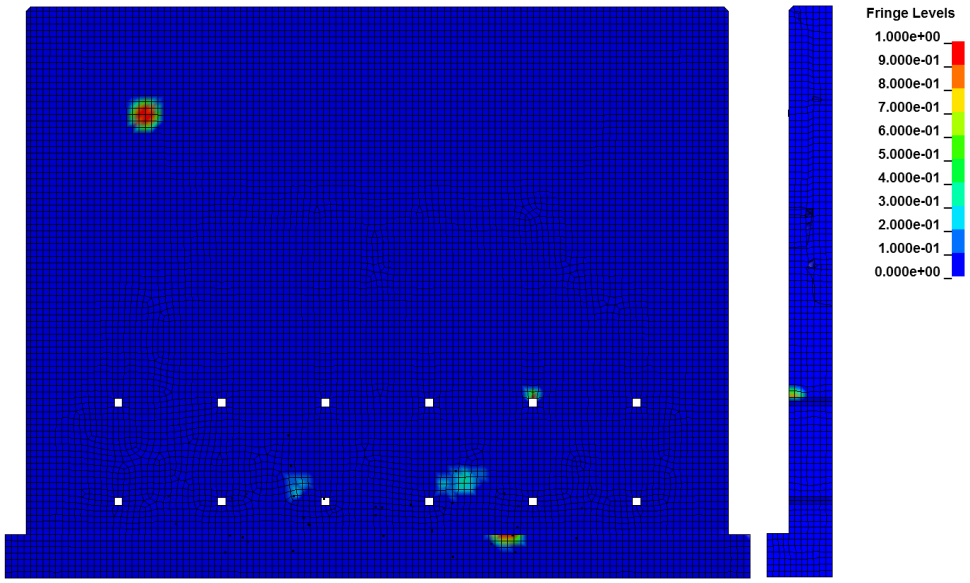

Figure 5.6.3 – Damage accumulation pattern in FullCrash35DS. At ground height and with additional deformation of the saferoom, the vehicle impact does not provoke spalling.

35-MPH ROOF IMPACT 20° TILTED (5.7)

For the full-scale roof impact, the saferoom was remeshed in order to have the mesh refinement in the roof instead of in the walls. Also the entire mesh was upgraded to a 100% hexaedron mesh. The new model, Figure 5.7.0, has 530,000 elements, 60,000 in the vehicle, 330,000 in the refined roof and 140,000 in the remaining of the saferoom/soil. Even with a higher number of elements, the structured mesh presented high quality, thus being more stable and accurate, while maintaining a running time equivalent to previous mesh. For this simulation, it was decided to tilt the vehicle by 20° to study a more realistic impact scenario.

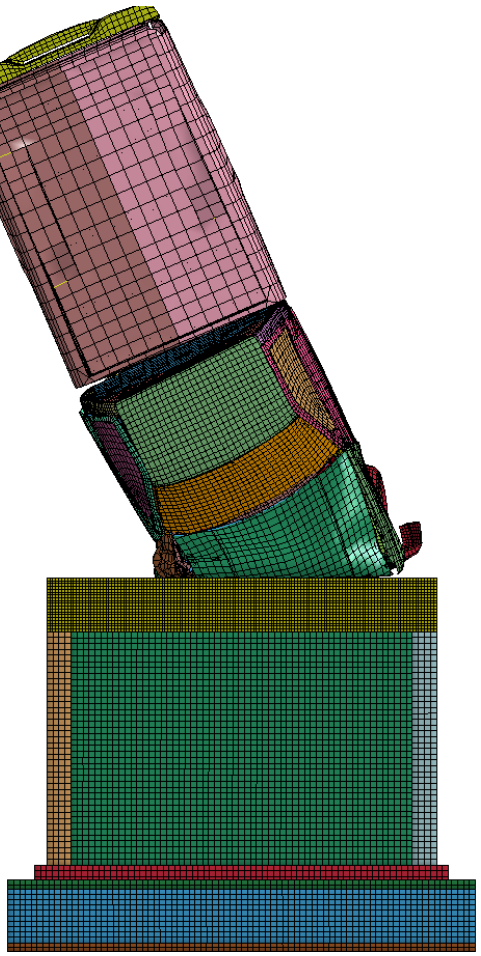

Figure 5.7.0 – Output of FullCrash35DRm25 at 0.085 s showing deformation of the vehicle.

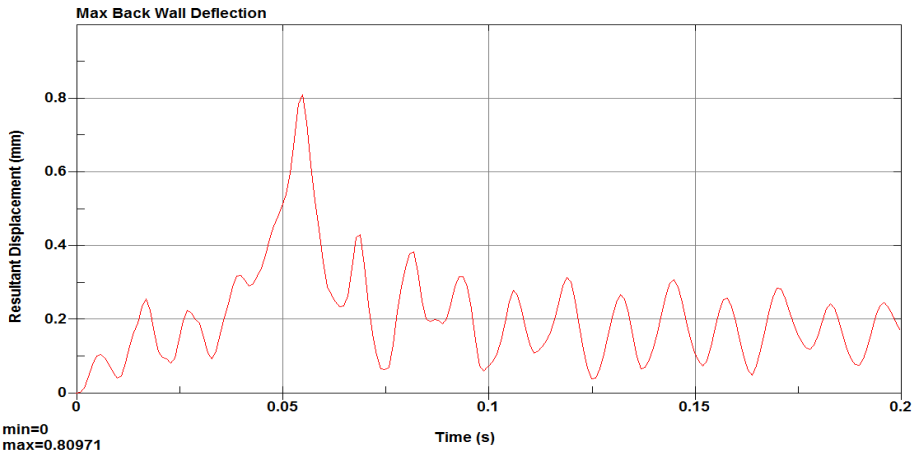

Figure 5.7.1 – FullCrash35DRm25 resultant nodal displacement with no filter applied. Note the impact peak caused by the engine block at .05 s and the roof natural frequency oscillations.

Figure 5.7.1 shows the displacement in the back face of the roof. The curve pattern resembles the RoofCrash35 run, and the maximum back-wall displacement has the same order of magnitude. Despite this similarity, frontal damage accumulation was much less severe. The maximum acceleration in Figure 5.7.2 (27.7 m/s^2) is equivalent to the SideCrash35D, the two simulations also share the best hourglass ratio among all simulations, which leads to assume acceleration levels of 25-30 m/s^2 as being the most accurate for a vehicle impact at 35 mph.

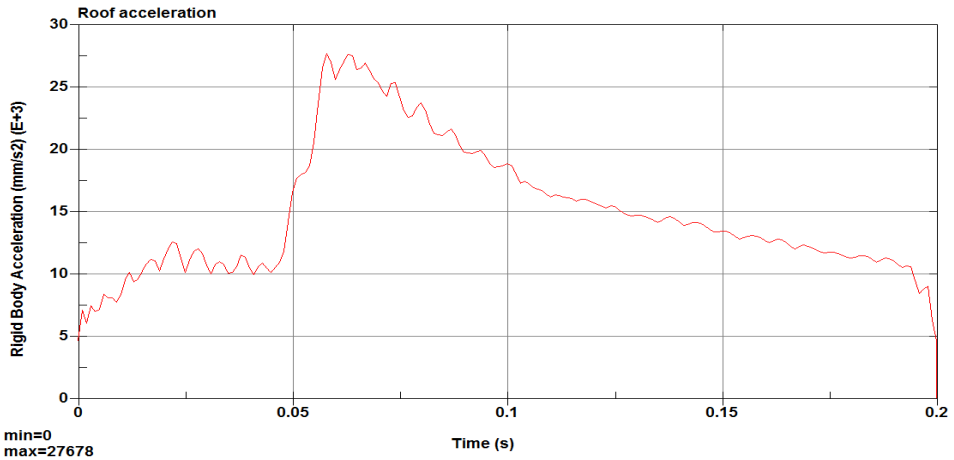

Figure 5.7.2 - Resultant acceleration for FullCrash35DRm25. Nine point data filtering applied to attenuate high-frequency noise.

The tilted pickup scenario is less severe than a frontal impact, as can be seen in Figure 5.7.3. The rotation of the vehicle widens the contact area, and prevents the engine block from hitting the roof. Given the nature of wind-accelerated trajectories, this scenario is much more likely than test 5.3.

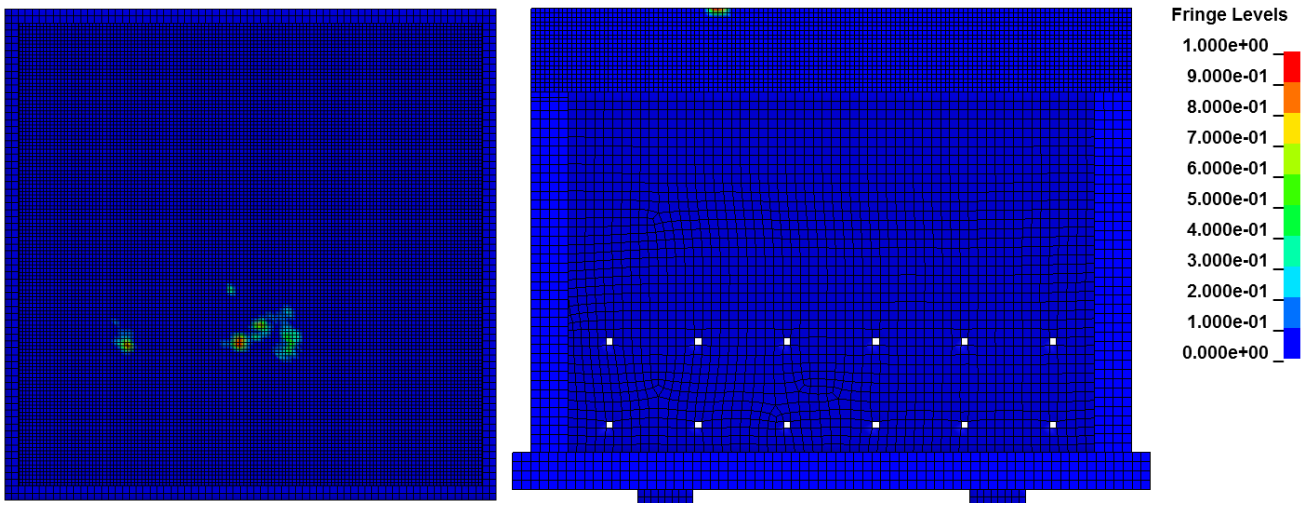

Figure 5.7.3 – Damage accumulation pattern in FullCrash35DRm25. Top view (left) and cross-section side view (right).

Another reason for the low damage is that the impact energy was not entirely absorbed – a portion of it was transformed into rotational energy as seen in Figure 5.7.4. This rotation will create a secondary impact as the car falls off the roof, but the effect was not captured since the simulation lasted for 0.2 seconds. In spite of that, the secondary crash will have minor effects due to the lower impact velocity and larger contact area.

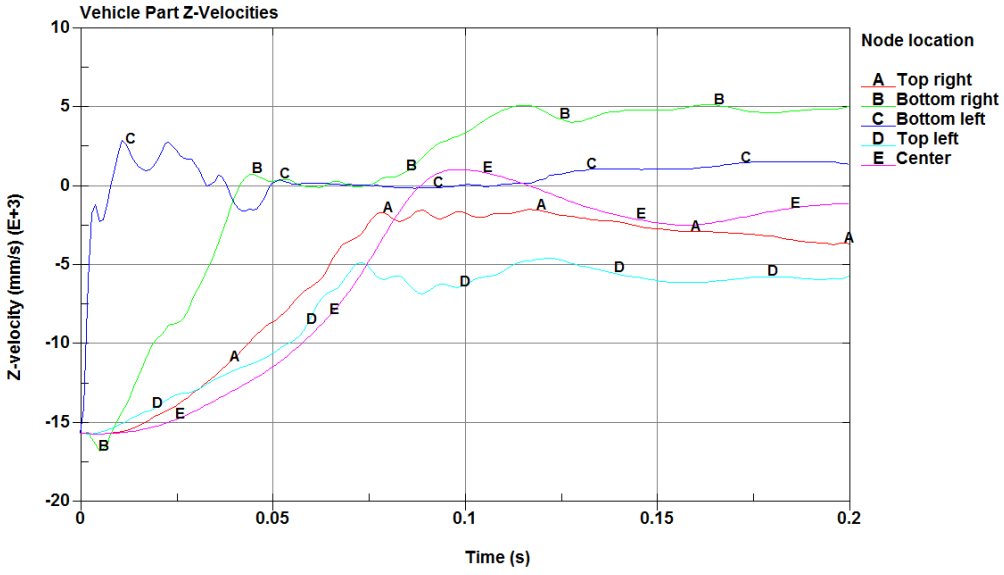

Figure 5.7.4 – Nodal velocities in 5 points of the vehicle in FullCrash35DRm25. Note that after the vehicle rebounds at ~.1 s, it continues to fall, and the velocities are nonzero. The center node serve as a reference for the center of mass; it has the smoothest profile.

35-MPH FRONT IMPACT (WORST CASE SCENARIO) (5.8)

The stability of the saferoom is dependent on the support of the side walls – an unconstrained concrete wall such as the front wall, is expected to develop higher stresses as compared to the other walls because of the free edge created by the door opening. To illustrate this effect, the vehicle model was impacted at the center of the front face of the saferoom. The model seen in Figure 5.8.0 shows the collision, the front wall has a refined mesh with 30,000 elements and 240,000 more elements in the other parts.

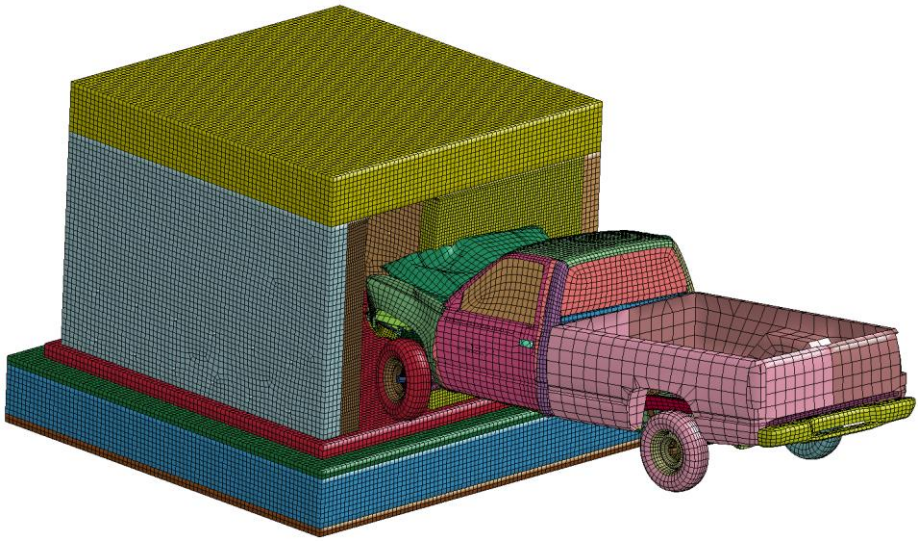

Figure 5.8.0 – Output of FullCrash35DF at 0.15 s. The deflection of the front slab is apparent, and damage is expected to be severe.

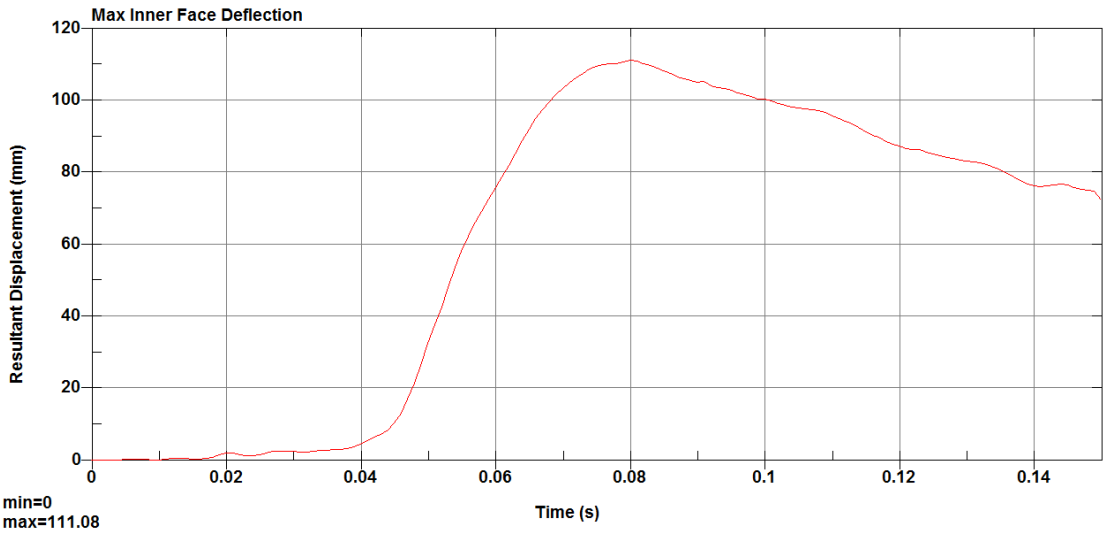

Figure 5.8.1 – FullCrash35DF resultant nodal displacement with no filter applied. Structure oscillations are masked by the high displacement value.

The displacement of the inner face of the front wall has a value of a 100 mm (Figure 5.8.1). This is much larger displacement compared to the previous impacts and indicates the formation cracks. The failure of the wall under this scenario can also be inferred from acceleration in Figure 5.8.2; the value is close to the value of the acceleration in test 5.4, where plug formation was also observed.

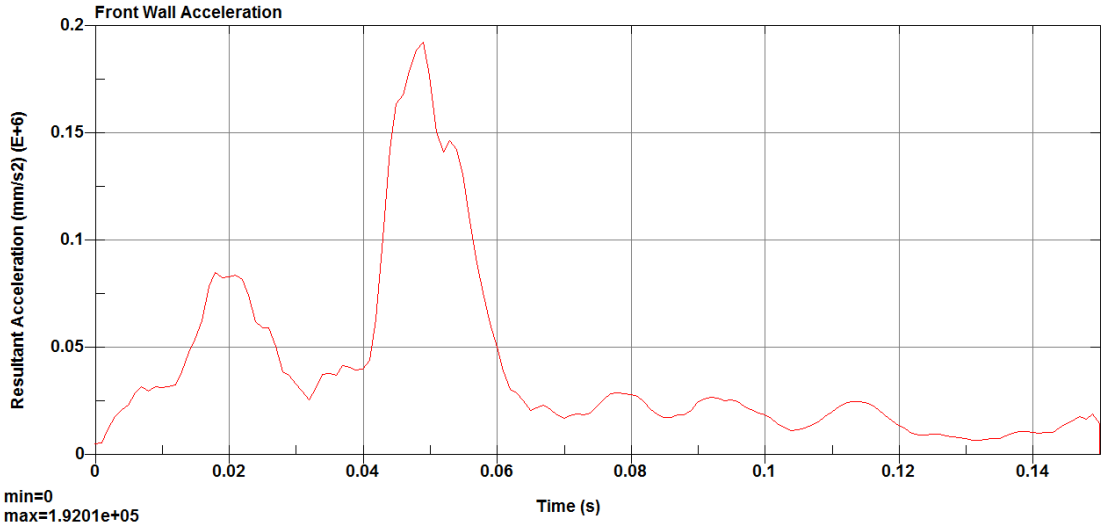

Figure 5.8.2 - Resultant acceleration for FullCrash35DF. High-frequency noise was attenuated.

Figure 5.8.3 shows fringe levels for the RHT damage variable. In this case the damage of the concrete extends through the thickness of the wall, which means that the inner surface of the wall will

experience cracking and possible spalling. It was observed that this damage is caused when the engine block contacts the wall directly. However as seen in figure 5.8.4 the simulation shows that the truck does not penetrate the wall.

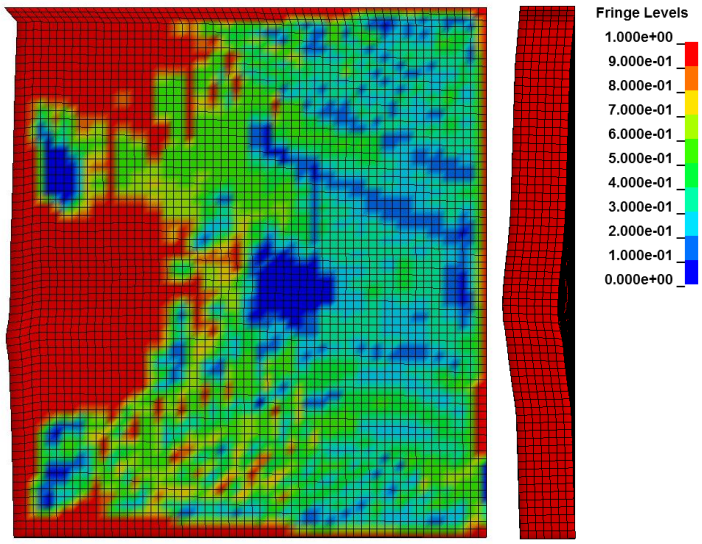

Figure 5.8.3 – Damage accumulation pattern in FullCrash35DF. The left region is the outer face of the Saferoom and the right region is the cross section of the wall at the impacted region.

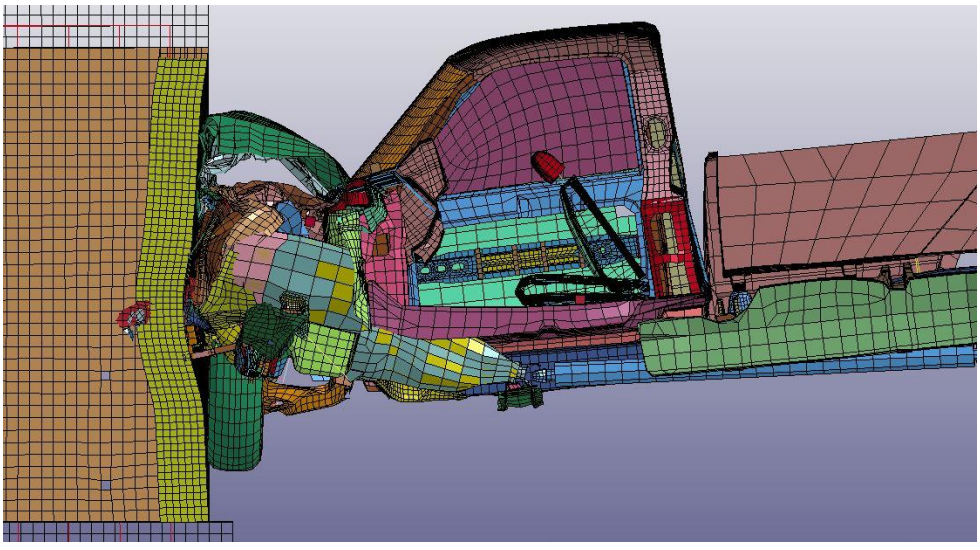

Figure 5.8.4 – Side view of the impacted front area showing large deformation of the inner surface but no penetration of the truck.

35-MPH ROLLING IMPACT 90° TILTED (5.9)

For the rolling impact, the saferoom model needed additional refinement. The vehicle would contact the saferoom along the entire length of the front wall, so a chamfer was applied to the corners to prevent erosion damage as seen in test series 3. The model is shown in Figure 5.9.0.

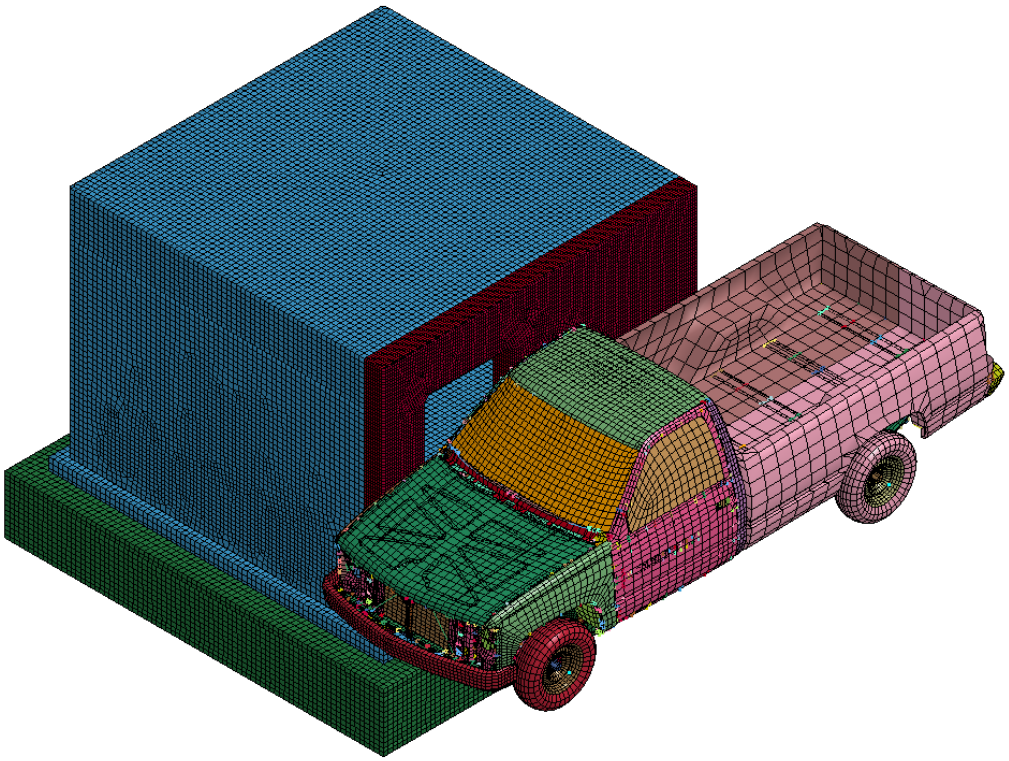

Figure 5.9.0 – Input of FullCrash35DF_90c, soil in green, saferoom in blue with refined mesh regions in red.

Figure 5.9.1 shows the behavior of the front wall under a side vehicle crash. There is considerable displacement since vehicles have poor performance in side collisions, therefore more energy is absorbed by the saferoom in the form of deformation. The small deformation of the side of the pickup also implies a higher acceleration, which is observed in Figure 5.9.2. Due to lower deflection, the impact occurs over 30ms, much faster than the 100ms impacts in the frontal crash tests.

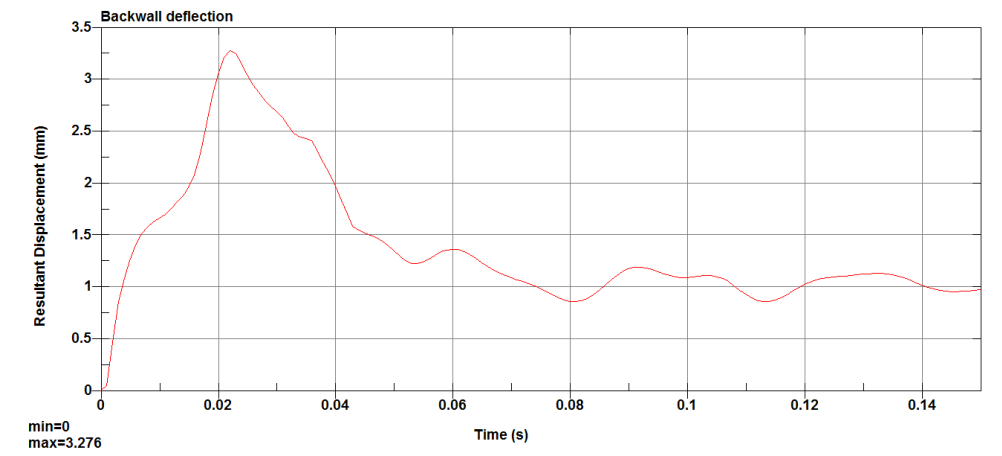

Figure 5.9.1 – FullCrash35DF_90c resultant nodal displacement. Data filtering applied to attenuate high-frequency noise.

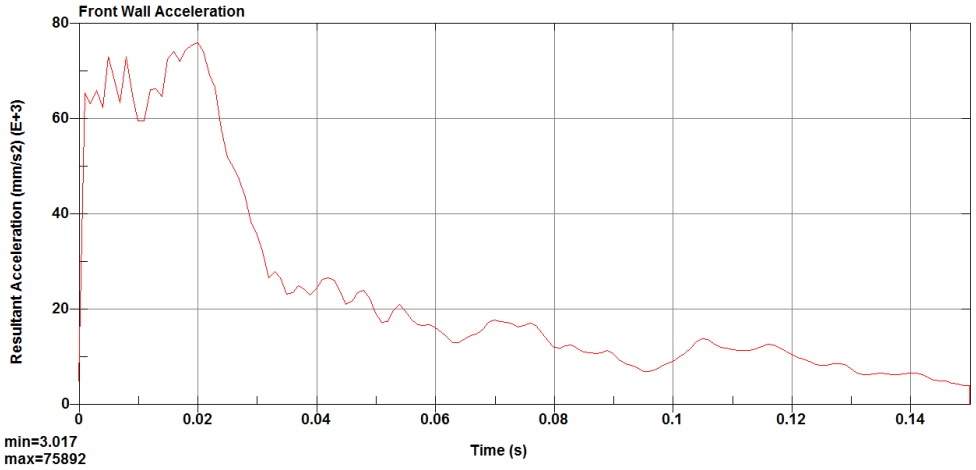

Figure 5.9.2 - Resultant acceleration for FullCrash35DF_90c, note the absence of a clear peak representing the engine block impact. High-frequency noise was attenuated.

The damage seen in Figure 5.9.3 is more distributed due to the bigger area of the side of the vehicle. Concentrated loading occurs in the corners, as was expected. The damage in the middle of the front wall has a depth of 20 mm, making it insignificant. However, the top right corner of the door clearly shows a shear cracking pattern caused by the collision of the upper part of the cabinet in the exact region where the front wall has an inner corner with the roof. The corner damage zones result from the impact of rigid parts such as the front brake assembly and the rear axle into the wall. The corner damage region extends deep into the structure, but is not indicative of penetration.

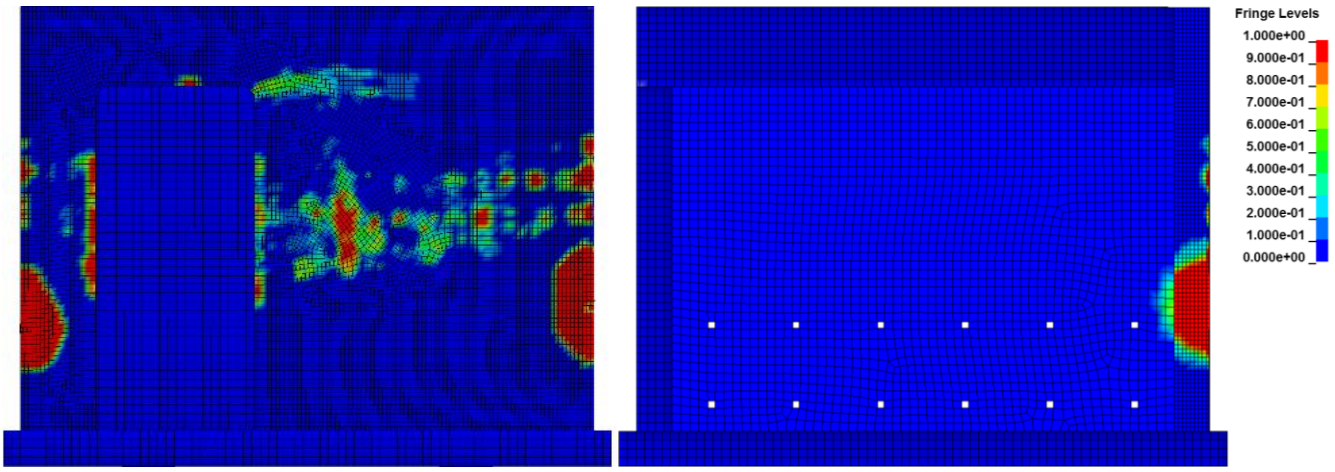

Figure 5.9.3 – Damage pattern in FullCrash35DF_90. Large damage zones on corners. Front and section view near right corner.

To capture realistic damage in the wheel region, it is necessary reformulate many of the suspension components of the car, which would require considerable time due to the number of parts and different materials. Also even those non-conservative results in the corners were not able to provoke penetration in the saferoom. Therefore the remodeling of the suspension was not pursued.

ANALYSIS

The full scale models permits deformation of the corner of the impacted wall which softens the impact and realistically transfers loads onto the remainder of the structure. This effect can especially be seen in the damage patterns of the last simulation. The structured model took from 8 to 17 hours to run, and represents the most accurate results with regard to parameters such as mesh convergence, hourglass energy and mass scaling. Considering the damage seen in the front wall impact, it is clear that it is the weakest side of the saferoom, and should be oriented away from any open spaces if possible. This way, the risk of a critical impact into the door region is reduced.

Conclusion

Approximately one hundred simulations were run to study various components of the OZ saferoom under impact. In this report, results from 32 simulations are presented.

In series 1 simulations we show how a slab section of the OZ saferoom performs under NSSA style impact tests. Additionally, we use series 1 tests to characterize wood and concrete material models. From these studies we concluded that the concrete used by OZ saferooms showed excellent resistance to soft impacts and has potential for damage absorbance from multiple impacts in the same zone. This implies OZ saferoom will be able to withstand direct impacts from several tornadoes without compromising structural integrity. We do not expected to see spallation until missile velocity exceeds 300 mph, which is not anticipated. Finally, we found that concrete performance is independent of temperature and moisture conditions in the environment.

Series 2 studied the same NSSA test with a steel projectile, trying to mimic the impact of an I-beam. From these tests we concluded that OZ saferooms offer significant protection against dense projectiles up to 45 mph, beyond that the risk of spallation increases but structure still withstands impact. No penetration was observed in these simulations.

To study the weaker points in saferoom structure we modeled and ran an NSSA-style test on the corner of OZ saferoom. No damage or penetration occurs up to 100 mph; at higher speeds external spallation and chipping occurs but the structural integrity is not compromised. We conclude that any damage to the corners will not affect the performance of the saferoom in subsequent tornadoes.

The final component of the saferoom to be studied in isolation was the door. We were able to show impact resistance from soft projectiles up to 100 mph. No bolts were dislodged under impact nor was penetration observed. Under impact of hard projectiles, or soft projectiles exceeding 100 mph, we expect more significant damage and recommend to have the door replaced.

Series 5 tests modelled a direct hit of the car into a full scale OZ saferoom. Although vehicles are complicated projectiles and predicting the damage pattern for every vehicle model at every angle and impact speed is impractical, we ran a series of simulations that studied the most significant impact scenarios. Based on these results we were able to progressively refine both the vehicle and structural mesh to obtain realistic results. We started with a reduced vehicle model and a single wall or roof model, and progressively moved towards more sophisticated geometry. In the full-scale tests, the saferoom was grounded in soil and not externally constrained. The results show that the saferoom will not tip over in vehicle crash impact scenarios.

For head-on impacts, damage occurs in select zones rather than uniformly. Particularly, the two bumper rails give a distinctive two-point damage pattern, followed by the fenders and the front-center of the hood. If the impact speed is high enough, there is a possibility the engine block will make contact with the concrete wall. A direct 35-mph impact is the only scenario in which spalling and damage may occur. The damage severity depends on the orientation of the saferoom, with the worst case occurring when the car impacts directly the center of the front face. Although it is highly unlikely that wind will accelerate a vehicle to that speed and orientation without inducing rolling along its major axis, the simulation provides realistic information in case of a moving vehicle collision. Therefore, orientation of the saferoom when considering placement near a road or highway is a practical consideration.

Additional vehicle crash scenarios were considered. For airborne vehicles, drop tests on the roof were simulated with 2 different vehicle orientations. Localized damage was observed and the acceleration of the roof was found comparable to previous experimental data. For the case of a rolling vehicle, a collision was simulated with the vehicle impacting along its side. The damage pattern was distributed with no penetration or peak deformation.

Based on these series of computer simulations, we demonstrate that the design of the OZ Saferoom is robust enough to protect its occupants during different impact loads experienced in an EF5 Tornado.

CLOSING COMMENTS

This finite element analysis is part of the assessment of the structural integrity and safety of the OZ saferoom. The most sophisticated software available for impact analysis, LS-DYNA, was used in this study, and proved to be an excellent tool for the computation and evaluation of saferoom impacts. Component simulations were run on a lab workstation, while full scale simulations were run on a high-performance computing cluster at the Rochester Institute of Technology. We recommend further work be conducted to validate the simulated findings experimentally. Additionally, future saferoom designs may require some further analysis to understand full-scale structural integrity.

ACKNOWLEDGEMENTS

The authors would like to extend their gratitude to OZ Saferooms for their generous support of this research program. Additional thanks to the Rochester Institute of Technology Depts. of Mechanical Engineering and Research Computing. Special thanks to William Finch and Paul Mezzanini, the sysadmins who installed LS-DYNA on the high-performance computing cluster. Thanks to Kathleen Ellis and Josh McSavaney, for moral and technical support throughout the course of the project.